BRAC UNIVERSITY

SCHOOL OF ENGINEERING AND COMPUTER SCIENCE

DEPARTMENT OF ELECTRICAL AND ELECTRONIC ENGINEERING

QUANTUM TRANSPORT IN NANOSTRUCTURED THERMOELECTRIC GENERATOR

BY

MOHAMMAD MOBASSAR HOSSAIN (12321036)

MD. SHARIF U ZZAMAN (12321041)

SHABAB AZFAR AHMED (12321018)

SHAFAT MD. SHAHRIAR (12321006)

IN PARTIAL FULFILMENT OF THE REQUIREMENT FOR THE DEGREE OF BACHELOR OF SCIENCE IN ELECTRICAL AND ELECTRONIC ENGINEERING

August, 2016

Dhaka, Bangladesh

BRAC UNIVERSITY

SCHOOL OF ENGINEERING AND COMPUTER SCIENCE

DEPARTMENT OF ELECTRICAL AND ELECTRONIC ENGINEERING

QUANTUM TRANSPORT IN NANOSTRUCTURED THERMOELECTRIC GENERATOR

BY

MOHAMMAD MOBASSAR HOSSAIN (12321036)

MD. SHARIF U ZZAMAN (12321041)

SHABAB AZFAR AHMED (12321018)

SHAFAT MD. SHAHRIAR (12321006)

IN PARTIAL FULFILMENT OF THE REQUIREMENT FOR THE DEGREE OF BACHELOR OF SCIENCE IN ELECTRICAL AND ELECTRONIC ENGINEERING

August, 2016

Dhaka, Bangladesh

CERTIFICATE

This is to certify that this thesis work entitled "Quantum Transport in Nanostructured Thermoelectric Generator " submitted by Mohammad Mobassar Hossain, Md. Sharif U Zzaman, Shabab Azfar Ahmed and Shafat Md. Shahriar is a bonafide thesis work carried out under my supervision and guidance and fulfilling the nature and standard required for the partial fulfillment of the degree of Bachelor of Science in Electrical and Electronic Engineering. The work embodied in this thesis has not been submitted elsewhere for a degree.

_____

(Prof. Dr. Mohammed Belal Hossain Bhuian)

Supervisor

Department of Electrical and Electronic Engineering

BRAC University

ACKNOWLEDGEMENTS

We are greatly indebted to our thesis supervisor Professor Dr. Mohammed Belal Hossain Bhuian and co-supervisor Mr. Atanu Kumar Saha for providing us with definite direction, professional guidance, constant encouragement from the beginning of the work and moral support in many ways during study period.

We are also greatly indebted to Mr. Annajiat Alim Rasel for his valuable assistance and direction to work in the BRAC University graphics lab and accomplish our goal.

We acknowledge the help, advice and guidance rendered by Head of the Electrical and Electronic Engineering Department, Dr. Sayeed Salam and Lecturer Mr. Avijit Das.

The support provided by Graphics Laboratory staff, Mr. Tauhidur Rahman, Md. Saddam Hossain and Department Coordinator of CSE department Mr. Golam Md. Zilani are unforgettable.

We are also grateful to all the peers of the B.Sc. Electrical and Electronic Engineering department. The cooperation and support of Mr. Shifur Rahman, Mr. Fatin Farhan Haque and Mr. Saber Ahmed are incomparable and indelible.

Last but not the least, we are obligated and grateful to Dr. Supriyo Datta for his book ‘Lessons from Nanoelectronics: A New Perspective on Transport’. It lifted our morale and unveiled the path for us in our research. It would not have been possible for us to carry out our indagation without his insightful knowledge regarding quantum transport.

ABSTRACT

In this study, we found thermoelectric figure of merit (ZT) at different room temperatures which performed better than conventional temperature. From a transition metal dichalcogenide material MoS_2 we got the highest ZT value of 4.392 at 300K. Besides this, in metal oxide such as ZnO gives the highest ZT value of 1.7108 at 310K. We have also studied Si-n Type, Si-p Type and SiGe which gives the value of ZT 2.405, 2.850 and 2.320 respectively at 300K.This study represents a bona fide study of thermoelectric materials accompanied by the modeling and simulations of an asymmetric thermoelectric device structure. The thermoelectric module will possess attributes such as a novel module design and a room temperature range rather than conventional high temperature modules. Electro-thermal interaction is commonly considered only as a matter of Joule heating. In addition, the Seebeck, Peltier and Thomson effects are significant in materials with high thermoelectric figure of merit ZT.

The materials that are currently being used by researchers in thermoelectric devices are semiconductors and metal-oxides. These materials include Sb_2Te_3, PbTe, Bi_2Te_3, $(BiSb)_2Te_3$, SiGe, Si; which are specifically developed for conventional and high temperature ranges. And from our study we have already said that there is another class of materials that are metal dichalcogenides(MoS_2) which have a good figure of merit(ZT) at room temperature. A high Seebeck coefficient α, a good electric conductivity σ and a poor thermal conductivity K are the characteristics of these materials. As a result, thermal and electrical performance of the thermoelectric module which represents a good electrical performance in thermoelectric generator.

Table of Contents

List of Figures

List of Tables

Abbreviations

BTE= Boltzmann Transport Equation

COP= Co-efficient of Performance

DFT= Density Functional Theory

MFP = Mean Free Path

MC = Monte Carlo

MD = Molecular Dynamics

NEGF = Non-Equilibrium Green's Function

NEMD= Non-Equilibrium Molecular Dynamics

TEG= Thermo-Electric Generator

Nomenclature

Constant:

K_B= Boltzmann constant, $1.38 \times 10^{-23}\ m^2 kgs^{-2}$

$\hbar$ = Reduced Planck constant, $1.055 \times 10^{-43}\ Js$

Symbols:

A= Cross-sectional Area, m^2

C= Spectral Volumetric Specific Heat, $Jm^{-3}Hz^{-1}K^{-1}$

D=Density of States per unit volume per unit frequency interval, $m^{-3}Hz^{-1}$

e= Charger Per Carrier, C

E_f = Fermi Level

E_g = Band Gap Energy

E_c = Conduction Band Energy

f_o = Fermi-Dirac Distribution

f_{BE}= Bose-Einstein Distribution

I= Electrical Current, A

J_e = Electrical Current Density, Am^{-2}

J_q= Heat Flux, Wm^{-2}

G_K= Thermal Conductance, $Wm^{-2}K^{-1}$

L=Transport Coefficients

Q= Heat Current, W

R= Electrical Resistance, Ω

S= Seebeck Co-efficient, VK^{-1}

T=Temperature, K

V= Velocity, ms^{-1}

Z= Figure of Merit, K^{-1}

B= Thomson Co-efficient, VK^{-1}

Π= Peltier Co-efficient

K= Thermal Conductivity, $Wm^{-1}K^{-1}$

$\emptyset$ = Co-efficient of Performance

ρ = Electrical Resistivity, Ωm

ω = Angular Frequency, rad. Hz

Chapter 1

1.0 Introduction:

According to the global energy consumption reports, among the total energy sources that are being used, 32% are from fossil fuel while 24% are from natural gas. However, these sources are depleting every day and cannot be depended upon forever. On the other hand, there are fields of solar energy and wind energy which have not been used as much as we would have wanted at 0.5% and 1% respectively. There are ongoing research going on by scientists from all around the world to develop these fields.

The global energy consumption at the current moment stands at around $4.1 \times 10^{20}\, J$ which is equivalent to 13 terawatts(TW) [1]. The projected population and economic grown by the end of this generation will more than triple the current global energy consumption rate [2]. The biggest challenge in supplying for the ever increasing demand of energy brings us to the problems like climate change. There is a constant search for new, clean and renewable energy sources which will be the prospects of the future. Among them, currently believed to be the most prominent of the renewable energies is the Solar energy [2]. If we compare them with the other energy sources such as the hydroelectric resource, wind power and the cumulative energy that can be gained from all tides and ocean currents in the world and the huge amount of solar energy that is available on this earth which needs to be exploited in order to meet the global energy demands of the world. When it comes to solar energy, it depends on the exploitation of three functional steps such as the capture, conversion and storage of the solar energy. As a result, high efficiency thermoelectric material is one of the most important research directions for solar power utilization.

The phenomenon of direct conversion of temperature difference to electric voltage and vice versa is known as the thermoelectric effect. The thermoelectric generator (TEG) can be used in conversion of heat generated by different sources such as radiation, automotive exhaust and industrial process to electricity. Again, refrigerators and other cooling systems can be made using the thermoelectric coolers. Since solid state devices are extremely high in reliability, they are widely used in infrared sensors, computer chips and satellites [1]. The only drawback in these thermoelectric devices in their low efficiency which can be again significantly improved.

Therefore, the improvement of thermoelectric efficiency has become the most key issue in the field of research.

The thermoelectric materials need to have a measurable quantity which we can related to its efficiency. The efficiency of thermoelectric materials to convert their energy is called the figure of merit [3,4], which is a function of several transport co-efficients:

$$ZT = \frac{S^2\sigma T}{K} = \frac{S^2 T}{K\rho} = \frac{S^2 T}{(K_e + K_l)\rho} \quad (1)$$

where S is the Seebeck co-efficient, σ and K are the electrical and thermal conductivity respectively. T is the absolute temperature, ρ is the electrical resistivity and thermal conductivity (K) of thermoelectric materials consists of two parts. They are namely the lattice thermal conductivity (K_l) and electronic thermal conductivity (K_e).

The maximum value of ZT as per the theoretical limit is infinity. That is there are no theoretical limits to the value of ZT. The best bulk thermoelectric materials that have been found so far are Bi_2Te_3, PbTe and SiGe. These materials have shown the maximum amount of ZT which is 1. [5] This restricts the large-scale application of thermoelectric technology. There have been significant progresses which have been made to improve the thermoelectric properties, especially recent achievements to create Nanostructure materials such as super lattices, nanowires and Nano-composites.

Even though there has been a very high anticipation and achievements, but the progress in the thermoelectric materials has still been limited. They have been limited to the current thermoelectric materials for practical applications. The thermoelectric materials which are being used commercially have a low ZT of 1 and the average thermoelectric generators available have a conversion efficiency of approximately 5%. There is a great potential for the discovery of materials whose ZT could range from 2-3 and this would provide a great conversion efficiency to be competitive with traditional mechanical energy conversion systems [5].

The increase of Seebeck coefficient is one of the major activities that is focused upon in thermoelectric materials. It also reduces the thermal conductivity of that material. There have been developments in bulk materials [6], Nano-scale materials [7,8,9] and bulk Nanostructured thermoelectric materials [10,11,12]. There have also been several developments that help us in

understanding the key feature of the influence of interfaces on thermoelectric performance [13] and theory of Nanostructure thermoelectric [14,15].

Here, in this paper we first discuss the basic principles and theory of thermoelectric effect. Then, we have discussed and studied different materials such as PGEC, Nanostructure and Nano-composite materials. We have also discussed the theory of electron and phonon transport in the thermoelectric materials. Applying these transport theories, we have been able to calculate the figure of merit for some discussed thermoelectric materials. Finally, we have discussed some popular TEGs structures and from them we have found out the electric potential, current density in these structures using our calculated values from material studies that we have conducted. As a result, we have been able to identify some new as well as established materials which could lead to the next generation of Nanostructured thermoelectric materials which will be further described in the analysis and discussion part.

Chapter 2

2.0 Thermoelectric Effect:

Thermoelectric effect is a process which include two major terms. One is conversion of temperature differences to electric voltage and another is electric voltage to temperature. In a thermoelectric device, if there is a temperature difference between the two sides of a metal then it creates an electrical potential difference between the two sides. On the other hand, if there is an applied voltage between the two sides of a metal then it creates a temperature difference.

For the rate of change of temperature and the direction of the change, a temperature gradient is established which causes the charge carriers in the material to diffuse from the high temperature side to low temperature side.

Thermoelectric effect includes three separately identified effects

(i) Seebeck Effect

(ii) Peltier Effect

(iii) Thomson Effect

2.1 Seebeck Effect:

The generation of electricity from a temperature difference at the junction of two different wires is known as the Seebeck effect. For the temperature difference, the electron energy level on the two sides are not in the same position so, the electron moves from high energy levels to the lower energy levels. This creates a magnetic field around the wire. This means current passes through the wire and creates a magnetic field around the wires. Due to electromotive force, there is a modification that happens in Ohm's law. Current is generated even when there is an absence of voltage difference or vice versa.

The local current density is given by,

$$J = \sigma\left(-\nabla V + E_{emf}\right) \tag{2}$$

Here V is the local voltage and σ is the local conductivity.

The Seebeck effect can be described as the creation of an electromotive field.

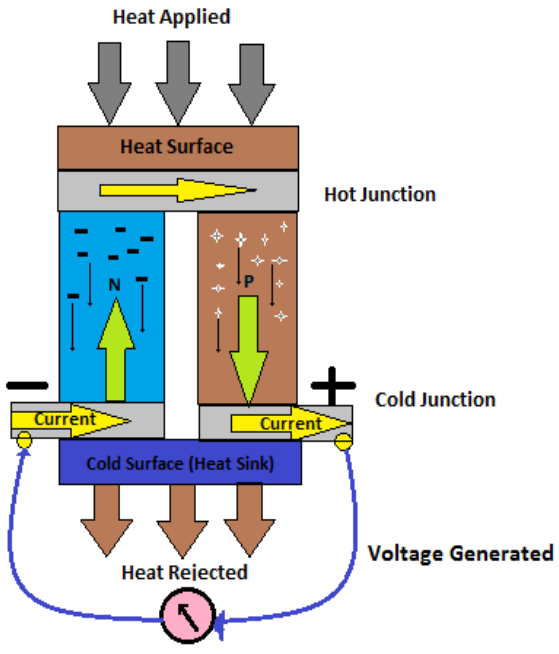

Figure 1. Seebeck Effect

$$E_{emf} = -S\Delta T \tag{3}$$

S is called the Seebeck coefficient. It is the property of the material used in the Seebeck effect. ∇T is known as the temperature gradients of in temperature T. The coefficients normally vary with respect to the temperature and on with what the conductor is composed of ordinary materials at room temperature have a Seebeck coefficient in the range of -100μV/K to 1000μV/K.

If the system reaches a steady state where J=0,

the voltage gradient is given simply by -SΔT-∇V = 0 then we can rewrite to,

$$-\nabla V = S\Delta T \tag{4}$$

This simple relationship which does not depend on conductivity is used in the thermocouple to measure a temperature difference. An absolute temperature may be found by performing voltage measurement at a known reference temperature. A metal of unknown composition can be classified by its thermoelectric effect if a metal of known composition is kept at a constant temperature. It is used commercially to identify metal alloys.

Thermocouples in series form a thermopile. Thermoelectric generators are used to create power from a heat differential.

2.2 Peltier Effect:

The Peltier effect is the presence of heating or cooling at an electrified junction of two different conductors. According to this theory, when a current is made to flow through a junction between two conductor A and B, heat may be generated at the junction. The Peltier heat generated at the junction per unit time Q, is equal to

$$Q = |\Pi_A - \Pi_B| I \tag{5}$$

Where Π_A, Π_B are the Peltier co-efficient of conductor A and B. I is the electric current from A to B. The total heat generated is not determined by the Peltier Effect alone, as it may also be influenced by the Joule heating and thermal gradient effects.

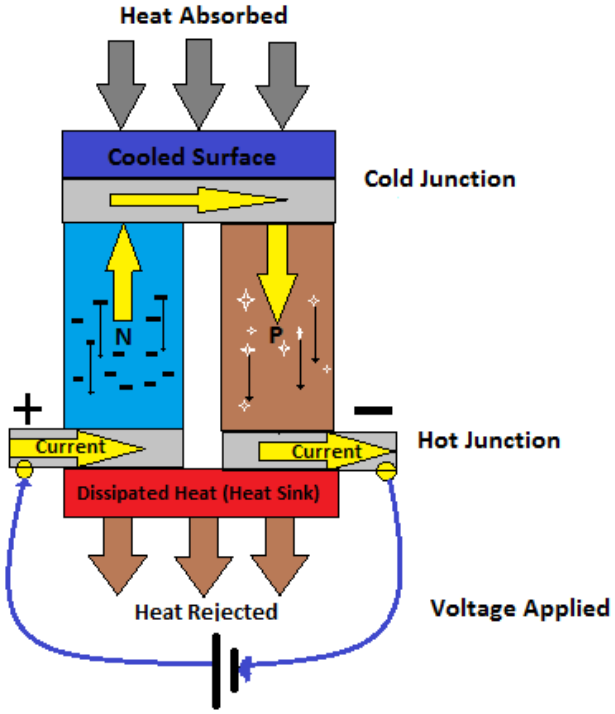

Figure 2. Peltier Effect

The Peltier coefficients represent how much heat is carried per unit charge. Since, charge current must be continuous across a junction, the associated heat flow will develop a discontinuity if Π_A, Π_B are different. The Peltier effect can be considered as the reverse of the Seebeck effect.

If a simple thermoelectric circuit is closed, then the Seebeck effect will drive a current which in turn will always transfer heat from the hot to the cold junction. The close relationship between the Peltier effect and Seebeck effect can be seen in the direct connection between their coefficients $\Pi_A = TS$.

A typical Peltier heat pump device involves multiple junctions in series, through which a current is driven. Some of the junctions lose heat due to the Peltier effect, while others gain heat. Thermoelectric heat pumps exploit this phenomenon, as do thermoelectric cooling devices found in refrigerators.

2.3 Thomson Effect:

In many materials, the Seebeck coefficient is not constant in temperature. So, a spatial gradient in temperature can result in a gradient in the Seebeck coefficient. If a current is driven through this gradient, then a continuous version of the Peltier effect will occur. The effect describes the heating or cooling of a current carrying conductor with a temperature gradient.

If a current density J is passed through a homogenous conductor, the Thomson effect predicts a heat production rate q per unit volume of

$$q = -KJ\,\nabla T \tag{6}$$

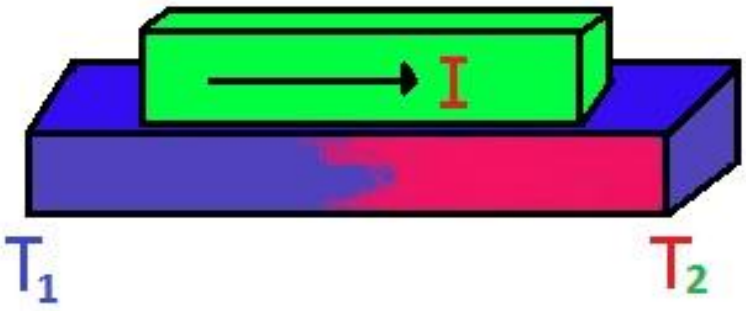

Figure 3. Thomson Effect

Here, ∇T is the temperature gradient and K is the Thomson coefficient. The Thomson coefficient is related to the Seebeck coefficient as, $K = T\,\frac{dS}{dT}$

This equation however, neglects Joule heating and ordinary thermal conductivity.

The field of thermoelectric is a potentially transformative power generation technology which has beenin practice for a long period of time due to their ability to convert heat directly in to electricity and to develop cost effective, pollution free forms of energy conversion.

Chapter 3

3.0 Material Study:

3.1 Background and History of Thermoelectric Materials:

The history of applications of thermoelectric materials is strongly associated with their efficiency. The early application of the thermoelectric effect is in metal thermocouples, which have been used to measure temperature and radiant energy for many years [16]. From the late 1950s, research on semiconducting thermocouples appeared, and semiconducting thermoelectric devices have been applied in terrestrial cooling and power generation and later in space power generation, due to their competitive energy conversion compared with other forms of small-scale electric power generators [16]. By the 1990s, many thermoelectric-based refrigerators can be found in the market, and starting around 2000, thermoelectric technology has been used to enhance the functions of automobiles such as thermoelectric cooled and heated seats [17]. The thermoelectric materials which had a figure of merit ($ZT<1$) were known for their low efficiencies. However, nowadays with the discovery of new materials whose ($ZT>1$) they can perform much more efficiently. For this reason, they are currently being utilized in the application of energy solutions.

3.2 Research Progress on Thermoelectric Materials:

1950:

In the 1950s, the basis of thermoelectric materials was widely well established. Materials such as Bi_2T_3, PbTe and SiGe bulk thermoelectric materials are called first generation materials. They were developed to work at room temperature, intermediate temperature and high temperature respectively.

1960:

The best method to improve figure of merit was to control the amount of doping as well as to form solid solutions. Solid solutions could be anything from Sb_2Te_3, PbTe-SnTe, etc. By increasing heat carrying phonons, point defects in solid solutions serve to decrease the lattice thermal conductivity.

Furthermore, there were also reductions in the charge carrier mobility and for this reason the enhancement of ZT was limited overall [9].

1960 to 1990:

$(Bi_{1-x}Sb_x)2(Se_{1-y}Te_y)_3$ family remained the best commercial material with ZT of about 1 in the field of thermoelectric materials during this time [18].

1990s:

The community of thermoelectricity was encouraged to do a reinvestigation for more advanced thermoelectric materials. These materials should have to have a high performance for thermoelectric power generation as well as cooling applications. As a result, there was a rebirth of interest regarding the development of these high-performance thermoelectric materials and their relevant theories. There were two methods that were being used as a convention to find the next generation of thermoelectric materials for the past two decades before this one. These approaches included finding and using new families of bulk thermoelectric materials which will have complex crystal structures. The other approach was synthesizing and using the low-dimensional thermoelectric materials system. The figure of merit has been significantly improved in these PGEC materials and Nanostructured materials. These materials include super lattices, quantum dots, Nano-wires and Nano-composite.

Though nanostructured materials have shown better performance for commercial use but there are other materials or way ,like Nano composite materials.There are two primary methodologies in searching for thermoelectric :

(i) Phonon glass electron crystal (PGEC) approach

(ii) Nano structuring of thermoelectric materials.

(i) Phonon glass electron crystal (PGEC):

An ideal thermoelectric material should be the combination of glass-like thermal conductivity and crystal-like electronic properties. This approach is the most achievable in materials with complex crystal structures, where voids (vacancies) and rattlers (heavy element atoms located in the voids)

would act as effective phonon scattering centers and reduce the lattice thermal conductivity significantly [19].

(ii) Nano structuring of thermoelectric materials:

The Nanostructuring of thermoelectric materials suggests that the ZT enhancement can be realized with nanoscale or nanostructured morphologies. Nanostructuring can improve the density of states(DOS) near the Fermi level via quantum confinement and therefore increase the thermopower. This provides a way to decouple thermos power and electrical conductivity.

Besides this, because the MFP (Mean Free Path) of electrons is much shorter than that of photons in heavily doped semiconductors, Nano structuring serves to introduce a large density of interfaces in which phonons over a large MFP range can be scattered more effectively and preferentially than electrons, as illustrated in Fig. 4. Hence, this will reduce the lattice thermal conductivity effectively while preserving carrier mobility and electronic conduction. This purpose can be achieved by preparation of nanostructures with one or more dimensions smaller than the MFP of phonons, while still larger than that of charge carriers [40].

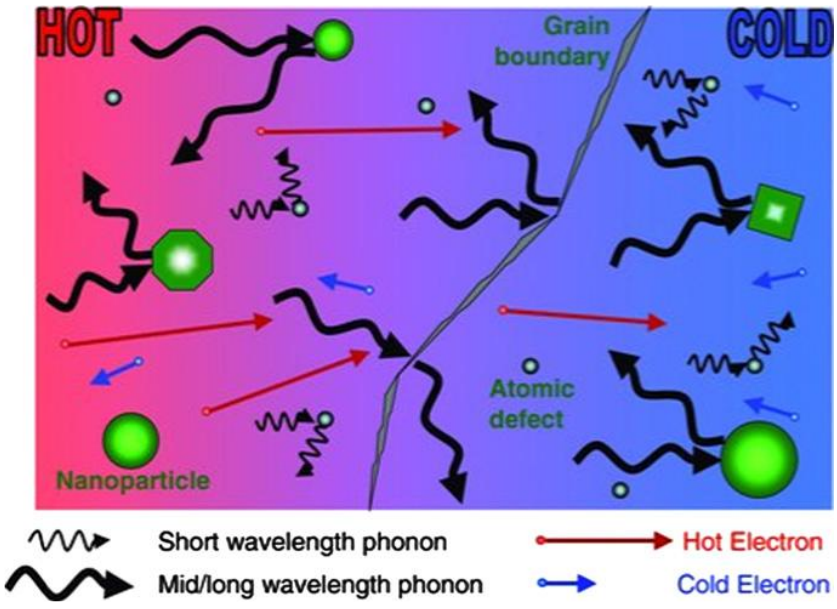

Figure 4. Schematic diagram illustrating phonon scattering mechanisms and electronic transport of hot and cold electrons within a thermoelectric material. (Taken from Fig.4 , [5])

3.3 Strategies Used to Improve Figure of Merit(ZT):

We will now discuss and review a few strategies that are used to improve the thermoelectric efficiency, which actually means the figure of merit for the thermoelectric performance. By increasing the electrical conductivity and Seebeck coefficient and decreasing the thermal conductivity we can see the direction in increasing the value of the figure of merit (ZT). However, it is not easy to improve ZT in reality because of the fact that σ, S, κ are all coupled with each other. The factors are also strongly dependent on the material's crystal structure, electronic structure and carrier concentration. Moreover, for a good thermoelectric material, not only is a high figure of merit over a wide operating temperature range required. Other than that, also sound mechanical, metallurgical and thermal characteristics to be used in practical thermoelectric generators.

3.4 Potential Thermoelectric Materials:

The electronic structure of a material influences the figure of merit of the material. Many materials can be simply classified into metals, semiconductors, and insulators according their electronic point of view. These three different classes of materials are characterized by zero, small and large band gaps, respectively. It can also be by free-charge-carrier concentration. The comparison of thermoelectric properties of metals, semiconductors and insulators at 300 K is shown in Table 1. We know that metals have very good electrical conductivity. However, the Seebeck coefficient of metals is very low (~5 $\mu V\ K^{-1}$). Metals also have large thermal conductivity which do not make them the most desirable materials for thermoelectric applications. Insulators have a large band gap, although they have large Seebeck coefficient (~1000 $\mu V\ K^{-1}$). Insulators also have extremely low electrical conductivity (~10- 12 $\Omega^{-1}\ cm^{-1}$) which results in a small value of $S^2\sigma$, and thus a small Z (~5×10-17 K^{-1}). These values are far smaller than that of metal (~3×10-6 K^{-1}). The optimal thermoelectric materials with a large value of $S^2\sigma$ is located in the region near the crossover between semiconductor and metal, with optimized carrier concentration of about 1×1019 cm^{-1}. The lattice thermal conductivity is assumed to be similar among these materials.

Table 1. Comparison of thermoelectric properties of metals, semiconductors and insulators at 300K. (after ref. [2])

Property	Metals	Semiconductors	Insulators
S ($\mu V\ K^{-1}$)	~ 5	~ 200	~ 1000
σ ($\Omega^{-1}\ cm^{-1}$)	~ 106	~ 103	~ 10-12
Z (K^{-1})	~3×10-6	~2×10-3	~5×10-17

3.5 What Kind of Band Structure Gives a Better Figure of Merit:

σ, S, K_e are determined by electronic band structure. Using the transport coefficients obtained by solving Boltzmann equation, and keeping all properties characterizing the material inside the transport distribution function $\sum(x)$, we obtain the expression of figure of merit.

$$ZT = \frac{\xi}{1 - \xi + A} \tag{7}$$

Where $\xi = \frac{I_1^2}{I_0 I_2}$, $A = \frac{1}{\alpha I_2}$. The dimensionless integrals I_n are defined as $I_n = \int dx \frac{e^x}{(e^x+1)^2} s(x) x^n$, and the dimensionless transport distribution function is given by $s(x) = \hbar a_0 \sum(\mu + x k_B T)$ which is measured from the chemical potential μ and scaled by the inverse temperature. There are two parameters $\alpha = \frac{\left(\frac{K_B}{e}\right)^2 T \sigma_0}{K_l}$ and $\sigma_0 = e^2/(\hbar a_0)$ which are determined by physical constants, where k_B is Boltzmann's constant, $\boldsymbol{e}$ the electronic charge, $\hbar$ the reduced Plank's constant, and a_0 the Bohr's radius. By analyzing Eqn. (7), it has been found that if the transport distribution takes the Dirac delta function, the figure of merit can be maximized. In other words, if electronic density of state near the chemical potential has a sharp singularity, the figure of merit can be very large. For example, assuming density of states has delta function, $N(\varepsilon) = n_i \delta(\varepsilon - b k_B T)$ with n_i being the concentration of energy levels, then the figure of merit can be expressed [21] as

$$(ZT)_{max} = 0.146 \frac{v d n_{i K_b}}{K_l} \tag{8}$$

where v is the group velocity of the carriers, d is the mean-free path. By choosing some typical parameters for a good thermoelectric material, the authors of Ref. [21] showed that a possible

figure of merit as high as ZT=14 can be obtained. Such high ZT is proposed to be achievable in rare-earth compounds. However, they also found that with a background added in the density of states, ZT is significantly reduced [21]. Therefore, the results obtained by Mahan and Sofo pointed to some new indications for searching for good thermoelectric materials:

(i) A very narrow distribution of energy carriers,

(ii) High carrier velocity in the direction of the applied electric field, and

(iii)Very small percentage ($< 1\%$) of background in density of states under a sharp peak.

3.6 Bravais Lattice:

There are 14 types of three-dimentional Bravais lattices. They are classified according to the length of their unit cell edges and also the angle they make with one another. We can take advantage of the symmetries of the lattice, and define the symmetry points in the Brillouin zone for instance for band structure calculations. The lattice must be constructed using the correct Bravais lattice class. The unit cell is categorized as triclinic.

Table 2. Bravais Lattice in Different Shape

System	Lengths and Angles	Number of Lattices
Cubic	a=b=c $\alpha = \beta = \gamma = 90^0$	3
Tetragonal	a=b≠c $\alpha = \beta = \gamma = 90°$	2
Orthorhombic	a ≠ b ≠c $\alpha = \beta = \gamma = 90°$	4
Rhombohedral	a=b=c $\alpha = \beta = \gamma \neq 90°$	1
Monoclinic	$a \neq b \neq c$ $\alpha = \gamma = 90° \neq \beta$	2

Triclinic	a $\neq b \neq$c $\alpha \neq \beta \neq \gamma$	1
Hexagonal	a $= b \neq c$ $\alpha = \beta = 90°$ $\gamma = 120°$	1

Chapter 4

4.0 Calculating Electrical Conductivity Using Transmission Spectrum Analysis:

The electronic properties of open and closed quantum systems which are based on density functional theory (DFT) are modeled using numerical basis sets.

The density matrix is the key parameter in this self-consistent loop. In case of the open quantum systems, the density matrix is calculated using the non-equilibrium Green's function also known as NEGF. Again, for the closed quantum systems or periodic systems the density matrix is calculated by diagonalization of the Kohn-Sham Hamiltonian. The electron density is defined by the Density Matrix while the effective potential is set up by the electron potential, i.e. the Hartree and exchange-correlation potential. The Kohn-Sham Hamiltonian can be obtained from the effective potential.

4.1.1 Kohn-Sham Hamiltonian:

In density functional theory (DFT), the system's electronic structure is described in terms of the one electron Kohn-Sham Hamiltonian.

$$\widehat{H}_{1el} = -\frac{\hbar}{2m}\nabla^2 + V^{eff}[n](\boldsymbol{r}) \tag{9}$$

The first term in the above equation describes the kinetic energy of the electron. The effective potential energy of the electron which is moving in the mean field from all the other electrons is described by the second term. The other electrons are described in terms of the total electron density n.

4.1.2 Solving the Kohn-Sham equations:

Now, by solving the one electron Schrodinger equation, we can find out the one-electron eigenstates of the Kohn-Sham Hamiltonian.

$$\widehat{H}_{1el}\Psi_\alpha(\boldsymbol{r}) = \varepsilon_\alpha\Psi_\alpha(\boldsymbol{r}) \tag{10}$$

In order to solve the differential equation, we have to expand the waves functions in a set of basis functions.

$$\Psi_\alpha(\boldsymbol{r}) = \sum_i a_{\alpha i}\,\phi_i(\boldsymbol{r}) \tag{11}$$

As a result, the differential equations are modified into a matrix equation from which we can determine $C_{\alpha i}$.

$$\sum_j H_{ij}\,C_{\alpha i} = \varepsilon_\alpha \sum_j S_{ij}\,C_{\alpha j} \tag{12}$$

The Hamiltonian matrix, $H_{ij} = \langle\phi_i|\,\widehat{H}_{1el}|\phi_j\rangle$, and overlap matrix, $S_{ij} = \langle\phi_i|\phi_j\,\rangle$ are given by 3D integrals over the basis functions.

4.1.3 Electron Density:

The electron density of the system is defined by the occupied eigenstates,

$$n(\boldsymbol{r}) = \sum_\alpha |\Psi_\alpha(\boldsymbol{r})|^2\, f\left(\frac{\varepsilon_\alpha - \varepsilon_F}{kT}\right) \tag{13}$$

where $f(x) = \frac{1}{(1+e^x)}$ is the Fermi function, ε_F the Fermi energy and T the electron temperature.

In terms of the density matrix, the density can be written as,

$$n(\boldsymbol{r}) = \sum_{ij} D_{ij}\phi_i(\boldsymbol{r})\phi_j(\boldsymbol{r}) \tag{14}$$

where the density matrix is given by basis set expansion coefficients,

$$D_{ij} = \sum_{\alpha} C^*_{\alpha i}\, C_{\alpha j} f\left(\frac{\varepsilon_\alpha - \varepsilon_F}{kT}\right) \tag{15}$$

4.1.4 Electron Difference Density:

The electron density is often convenient to compare to the superposition of atom based densities, $n^{atom}(\boldsymbol{r} - \boldsymbol{R_\mu})$, where $\boldsymbol{R_\mu}$ is the position of atom $\boldsymbol{\mu}$. Δn is called the electron difference density.

$$\Delta n(\boldsymbol{r}) = n(\boldsymbol{r}) - \sum_{\boldsymbol{\mu}} n^{atom}(\boldsymbol{r} - \boldsymbol{R_\mu}) \tag{16}$$

4.1.5 Effective Potential:

There are three contributions in Effective Potential:

$$V^{eff}[n] = V^H[n] + V^{xc}[n] + V^{ext} \tag{17}$$

In this equation, the first two terms show the interaction between the other electrons and this is represented through the electron density. The first term, $V^H[n]$, is the Hartree potential which occurs due to the mean-field electrostatic interaction. The second term, $V^{xc}[n]$, which is caused by the quantum mechanical nature of the electrons is the exchange-correlation potential.

V^{ext}represents any other electrostatic interaction that takes place in the system. The contributions from the ions potentials and the electrostatic interaction with an external electrostatic field can be represented by it.

4.1.6 External Potential:

The external potential is given by the pseudo-potentials and an external electrostatic field. This field may arise from the inclusion of metallic gates

$$V^{ext} = \sum_{\boldsymbol{\mu}} V_{\boldsymbol{\mu}}^{pseudo} + V^{gate} \tag{18}$$

The pseudo potential has two contributions,

$$V^{pseudo} = V^{local} + \sum_{n\,,\;n'} \left|X_n\right\rangle B_{n,n'} \left\langle X_{n'}\right| \tag{19}$$

where the first part is a local interaction and the last part is a non-local interaction. Due to the non-local part of the pseudo-potential, the range of the Hamiltonian is longer than twice the interaction range of the basis functions.

The V^{gate} is the electrostatic potential from the external gates calculated with zero electron density.

4.1.7 Hartree Potential:

We can calculate the electrostatic potential from the electron charge density. So the Hartree potential must be calculated from the Poisson equation.

$$\nabla^2 V_H[n](\boldsymbol{r}) = -4\pi n(\boldsymbol{r}) \tag{20}$$

The Poisson equation is a second-order differential equation. A boundary condition is therefore required to fix this solution. The molecular systems have the boundary condition that the potential goes asymptotically to zero. The boundary condition is that the potential is periodic in bulk system.

4.1.8 Exchange-Correlation Potential:

In DFT, the exchange-correlation energy includes the quantum mechanical effect of the other electrons. There are different approximations that are available for the exchange-correlation energy.

The exchange-correlation potential can be derived from the exchange-correlation energy, and is a mean-field quantum mechanical interaction potential between the electrons

$$V^{xc}[n](\boldsymbol{r}) = \frac{\delta E^{XC}}{\delta n}(\boldsymbol{r}) \tag{21}$$

4.1.9 Total Energy and Forces:

In DFT, the total energy is a functional of the electron density n and given by

$$E[n] = T[n] + E^{xc}[n] + E^{H}[n] + E^{ext}[n] \tag{22}$$

Where $T[n]$ is the kinetic energy of the Kohn-Sham orbitals,

$$T[n] = \sum_{\alpha} \langle \Psi_{\alpha} \left| -\frac{\hbar}{2m}\nabla^2 \right| \Psi_{\alpha} \rangle \, f\left(\frac{\varepsilon_{\alpha} - \varepsilon_F}{kT}\right) \tag{23}$$

$E^{xc}[n]$ is the exchange-correlation energy, $E^{H}[n]$ is the Hartree energy and $E^{ext}[n]$ is the interaction energy with the pseudo potential ions and other electrostatic external potentials.

The forces are calculated by differentiating the total energy with respect to the ionic coordinate of atom i at position $\boldsymbol{R}_i$

$$\boldsymbol{F}_i = -\frac{dE[n]}{d\boldsymbol{R}_i} \tag{24}$$

4.1.10 Local Atomic Orbitals(LCAO) Basis Set:

The electronic structure is expanded in a basis of local atomic orbitals (LCAO's)

$$\phi_{nlm}(\boldsymbol{r}) = R_{nl}(\boldsymbol{r})Y_{lm}(\hat{\boldsymbol{r}}) \tag{25}$$

where Y_{lm} is a spherical harmonic and R_{nl} is a radial function with compact support i.e. exactly zero outside a confinement radius.

4.1.11 Initial Spin:

Both collinear and non-collinear calculations may have different local minima spin configurations. It is important to prepare the system in the correct initial spin configuration such that self-consistent calculation will end up in the lowest energy spin configuration. The initial spin direction on each atom is specified in physical spherical coordinates (r, θ, ϕ), where θ is the angle with the z axis, and ϕ the polar angle in the x-y plane relative to the x-axis. The collinear case is $\theta = 0\ or\ \pi$ Radians [25].

4.1.12 Local Density Approximation (LDA):

In LDA the exchange-correlation functional is taken as a function of the local density

$$E^{LDA}[n] = \int n(r)\, \varepsilon^{LDA}\big(n(r)\big) dr \qquad (26)$$

where $\varepsilon^{LDA}\big(n(r)\big)$ is the exchange-correlation energy density of a homogeneous electron gas with density $n(r)$.

It is possible to calculate the exact exchange energy for the homogeneous electron gas, the so-called Dirac-Bloch exchange energy, which is used for all LDA functions. The correlation energy cannot be calculated exactly. A number of different approximations exists. Most of them give almost identical results; the most commonly used variant is the parametrization by Perdew and Zunger.

4.1.13 U mean-field Hubbard Term:

The local approximations to the exchange-correlation energy has a number of short comings, where the most important are

- Self-interaction, an electron interacts with itself and this prevents electrons from localizing.

- Poor approximation for excited states, band gaps are often too low.

The mean field Hubbard correction, popularly called LDA+U or XC+U, is a semi-empirical correction which tries to improve on these deficiencies of the local exchange-correlation functions. [23,24]

In the XC+U an additional energy term,

$$E_U = \frac{1}{2}\sum_{\boldsymbol{\mu}} U_{\boldsymbol{\mu}} \left(n_{\boldsymbol{\mu}} - n_{\boldsymbol{\mu}}^2\right) \tag{27}$$

is added to the Exchange- Correlation energy. In this equation $n_{\boldsymbol{\mu}}$ is the projection onto an atomic shell and $U_{\boldsymbol{\mu}}$ is the "Hubbard U" for that shell. The E_U energy term is zero for a fully occupied or un-occupied shell, while positive for a fractional occupied shell.

The energy is thereby lowered if states become fully occupied or empty. This may happen if the energy levels move away from the Fermi Level, i.e. increasing the band gap, or if the broadening of the states is decreased, i.e. the electrons are localized. Thus, the Hubbard U improves on the deficiencies of the local exchange-correlation functional listed above.

The value of U is often used as an empirical parameter which is varied in order to improve the comparison between DFT and experimental data. However, it has also been suggested that the value of U is obtained by minimizing the total energy of the system.

Some caution must be taken when using the XC+U correction, since for large U values the electron density may have several local minima where some of them are unphysical, and it is often necessary to select an anisotropic initial electron state to reach the correct local minimum.

4.1.14 Onsite Representation:

In the onsite representation the local occupation matrix is given by

$$n^{\sigma}_{\boldsymbol{\mu},\boldsymbol{mm'}} = D^{\sigma}_{\boldsymbol{\mu m},\boldsymbol{\mu m'}} \tag{28}$$

where D is the density matrix, μ a basis orbital index and σ a spin index.

4.1.15 Onsite Shell Representation:

In the onsite shell representation, the occupation is obtained by summing together all the basis functions in each angular momentum shell, l

$$n^{\sigma}_{l,mm'} = \sum_{\mu \epsilon l} n^{\sigma}_{\mu,mm'} \tag{29}$$

4.1.16 Dual Representation:

In the dual representation the local occupation matrix is given by

$$n^{\sigma}_{\boldsymbol{\mu,mm'}} = \sum_{i,n}\left[S_{\mu m,in} D^{\sigma}_{in,\mu m'} + D^{\sigma}_{\mu m,in} S_{in,\mu m'}\right] \tag{30}$$

where S is the overlap matrix.

Dual Shell representation:

Similar to the Onsite Shell, the Dual Shell occupation is obtained by summing together all dual occupations in each angular momentum shell l

$$n^{\sigma}_{\boldsymbol{l,mm'}} = \sum_{\mu \epsilon l} n^{\sigma}_{\boldsymbol{\mu,mm'}} \tag{31}$$

4.2 Calculating Thermal Conductivity Using Phonon Transmission Analysis:

The road to understand heat conduction in crystalline solids started when the quantum theory of lattice vibration was developed and as a result, the phonon concept was established. The Einstein model and Debye model based on Planck's quantization, were able to point the temperature dependence of the lattice specific heat. Which leads to the harmonic oscillator model and corresponding Bose-Einstein distribution for the lattice vibration, in other words phonon. If we consider ideal cases, interatomic potential creates an infinite thermal conductivity. But in a real crystal, the anharmonic part in interatomic potential creates scattering among phonons, resulting a finite thermal conductivity. This scenario can be divided in two sets. It will be either a normal process which conserves crystal momentum or an Umklapp process which does not. Now, the

Umklapp process creates a resistance to heat flow while the normal process only redistributes phonons. Peierls extended the Boltzmann formulation for phonon transport taking the Umklapp process for phonon scattering into account [3]. Callaway further customized the theory taking both the normal and Umklapp scattering processes in account [4]. His assumption was that normal processes lead to a displaced Bose-Einstein distribution and ultimately affecting the Umklapp processes. So, by now we can easily recognize that Boltzmann transportation theory plays a very important role in understanding heat flow and phonon scattering within any thermoelectric device.

4.2.1 Boltzmann Equation:

The Boltzmann equation in the presence of a temperature is:

$$\left(\frac{\partial N}{\partial t}\right) - c.\nabla T\frac{dN}{dT} = 0 \tag{32}$$

Where N is the distribution function, T the temperature, c the group velocity, and $\frac{\partial N}{\partial t}$. the rate of change of N due to collisions. Now replacing $N\ by\ N_0$, the Planck distribution function:

$$\left(\frac{\partial N}{\partial t}\right) = \frac{N(\lambda) - N}{\tau_N} + \frac{N_0 - N}{\tau_u} \tag{33}$$

$\tau_N$to be the relaxation time for all normal processes and $\tau_u$to be the relaxation time for those processes. If we define $n_1 = N - N_0$ the Boltzmann (32) can be written as

$$-\frac{\hbar\omega}{KT^2}c.\nabla T\frac{e^{\frac{\hbar\omega}{KT}}}{\left(e^{\frac{\hbar\omega}{KT}}-1\right)^2} + \frac{\lambda.K}{\tau_N KT}\frac{e^{\frac{\hbar\omega}{KT}}}{\left(e^{\frac{\hbar\omega}{KT}}-1\right)^2} - \left(\frac{1}{\tau_N}+\frac{1}{\tau_u}\right)n_1 = 0 \tag{34}$$

The phonon specific heat C_{Ph} is:

$$C_{Ph} = \frac{\hbar^2\omega^2}{KT^2}\frac{e^{\frac{\hbar\omega}{KT}}}{\left(e^{\frac{\hbar\omega}{KT}}-1\right)^2}$$

Using $\tau_c^{-1} = \tau_N^{-1} + \tau_u^{-1}$ and $n_1 = -\alpha c.\nabla T\frac{\hbar\omega}{KT^2}\frac{e^{\frac{\hbar\omega}{KT}}}{\left(e^{\frac{\hbar\omega}{KT}}-1\right)^2}$ in (3)

$$\frac{\hbar\omega\alpha}{\tau_c T} c.\nabla T \frac{\lambda.K}{\tau_N} = \frac{\hbar\omega}{T} c.\nabla T \tag{35}$$

Since λ must be a constant vector in the direction of the temperature gradient, it is convenient to define a parameter β with the dimensions of a relaxation time by

$$\lambda = -\left(\frac{\hbar}{T}\right)\beta c^2 \nabla T \tag{36}$$

Since $k = c\omega/c^2$, we have

$$\lambda.k = -\left(\frac{\hbar\omega}{T}\right)\beta c.\nabla T, \tag{37}$$

so that (9) simplifies:

$$\frac{\alpha}{\tau_c} - \frac{\beta}{\tau_N} = 1, or\ \alpha = \tau_c\left(1 + \frac{\beta}{\tau N}\right) \tag{38}$$

if we make use of the isotropy, the thermal conductivity is found to be:

$$K = \frac{c^2}{2\pi^2}\int \tau_c\left(1 + \frac{\beta}{\tau_N}\right) C_{Ph} k^2 dk \tag{39}$$

$$\beta = \frac{\int_0^{\frac{\theta}{T}} \frac{\tau_c}{\tau_N}\frac{e^x}{(e^x-1)^2} x^4\, dx}{\int_0^{\frac{\theta}{T}} \frac{1}{\tau_N}\left(1 - \frac{\tau_c}{\tau_N}\right)\frac{e^x}{(e^x-1)^2} x^4 dx} \tag{40}$$

4.2.2 Calculation of The Thermal Conductivity:

The extreme simplification in this model does not appear possible to evaluate the basic integrals. The theory is temperature dependence. The thermal conductivity is obtained from (39) and (40) employing the relaxation times discussed in the introduction. We can write,

$$\tau_u^{-1} = A\omega^4 + B_1 T^3 \omega^2 + \frac{c}{L} \tag{41}$$

$A\omega^4$ represents the scattering by point impurities or isotopes, $B_1T^3\omega^2$ includes the umklapp processes$\left(B_1 = e^{\frac{\theta}{\alpha T}}\right)$ and $\frac{c}{L}$ is the boundary scattering. The thermal conductivity of germanium has been made on a sample almost isotopically $pure$,[5] now for A=0 Similarly

$$\tau_N^{-1} = B_2T^3\omega^2 \tag{42}$$

where B2 is independent of temperature. The combined relaxation time is

$$\tau_e^{-1} = A\omega^4 + (B_1 + B_2)T^3\omega^2 + \frac{c}{L}, \tag{43}$$

Then

$$K = \frac{K}{2\pi^2 c}(I_1 + \beta I_2), \tag{44}$$

Where

$$I_1 = \int_0^{\frac{K\theta}{\hbar}} \tau_c \frac{\hbar^2\omega^2}{K^2T^2} \frac{e^{\frac{\hbar\omega}{KT}}}{\left(e^{\frac{\hbar\omega}{KT}} - 1\right)^2}\omega^2 d\omega. \tag{45}$$

and

$$I_2 = \int_0^{\frac{K\theta}{\hbar}} \frac{\tau_c}{\tau_N} \frac{\hbar^2\omega^2}{K^2T^2} \frac{e^{\frac{\hbar\omega}{KT}}}{\left(e^{\frac{\hbar\omega}{KT}} - 1\right)^2}\omega^2 d\omega. \tag{46}$$

I_1, Introduce the dimensionless variable x, (45) becomes, on substitution of (43)

$$I_1 = \left(\frac{KT}{\hbar}\right)^3 \int_0^{\frac{\theta}{T}} \frac{x^4}{\left(Dx^4 + Ex^2 + \frac{c}{L}\right)} \frac{e^x}{(e^x - 1)^2} dx \tag{47}$$

After first order

$$I_1 = \frac{4\pi^4}{15}\frac{L}{c}\left(\frac{KT}{\hbar}\right)^3 \left[1 - \frac{20\pi^2}{7}\frac{EL}{c} - 16\pi^4\frac{DL}{c}\right],$$

which gives rise to a thermal conductivity (neglecting the βT_2 term).

$$I_1 = \frac{2K\pi^4}{15}\frac{L}{c^2}\left(\frac{KT}{\hbar}\right)^3\left[1 - 16A\left(\frac{\pi KT}{\hbar}\right)^4\frac{L}{c} - \frac{20}{7}(B_1 + B_2)T^3\left(\frac{\pi KT}{\hbar}\right)^2\frac{L}{c}\right], \qquad (48)$$

For, the strong dependence of D and E on the temperature, at higher temperatures the situation is reversed, and c/L is effectively small. If D is large, the isotope scattering is very effective for short waves and we may evaluate (22) approximately by replacing $\frac{\boldsymbol{x^2e^x}}{\boldsymbol{(e^x-1)^2}}$ by unity. At temperatures above perhaps $30K$ and using Binomial expansion:

$$I_1 = \frac{\pi}{2}\frac{1}{[A(B_1 + B_2)]^{\frac{1}{2}}T^{\frac{1}{2}}}\left[1 - \frac{\left(\frac{cA}{L}\right)^{\frac{1}{2}}}{(B_1 + B_2)T^3}\right] \qquad (49)$$

If we anticipate βI_2 in (44) small correction will be proved, from (24) that the thermal conductivity in the region just beyond the Iow-temperature maximum will be proportional to $T^{1/2}$, $(B_2 \ll B_1)$ temperature dependence $\boldsymbol{e^{\frac{\theta}{2aT}}}$ will be observed. If A is very small, then a chemically pure single crystal containing only one isotope. We cannot use the isotope contribution then if we set D=0 in (47)

$$I_1 = \left(\frac{KT}{\hbar}\right)^3\frac{1}{E}\int_0^{\frac{\theta}{T}}\frac{x^4}{x^2 + \frac{c}{LE}}\frac{e^x}{(e^x - 1)^2}dx \qquad (50)$$

If we shall retain the finiteθ/T. Even at temperatures for which the boundary scattering may still be regarded as small, (25) does not possess an expansion in integral powers of c/LE. A reasonable approximation is:

$$I_1 = \left(\frac{KT}{\hbar}\right)^3\frac{1}{E}\left[\frac{1}{3}\pi^2 - e^{-\frac{\theta}{T}}\left(\frac{\theta^2}{T^2} + \frac{2\theta}{T} + 2\right) - \frac{\pi}{2}\left(\frac{c}{LE}\right)^{\frac{1}{2}}\right]$$

$$= \frac{K\pi^2}{3\hbar(B_1 + B_2)T^2}\left\{1 - \frac{3e^{-\frac{\theta}{T}}}{\pi^2}\left(\frac{\theta^2}{T^2} + \frac{2\theta}{T} + 2\right) - \frac{3\hbar}{2\pi KT^{\frac{1}{2}}}\left[\frac{c}{L(B_1 + B_2)}\right]^{\frac{1}{2}}\right\} \qquad (51)$$

The thermal conductivity in isotopically pure materials should depend on temperature as T^{-2} which is beyond the low-temperature maximum. However, the size dependence is relatively less important in The isotopically pure material as the over-all conductivity is higher. We must calculate relatively small effect. This will not be valid at very low temperatures. For normal material,

$$\frac{\tau_c}{\tau_N} = B_2 T^3 \omega^2 / \left[A\omega^4 + (B_1 + B_2)T^3\omega^2 + \frac{C}{L}\right],$$

$$I_2 = B_2 T \left(\frac{KT}{\hbar}\right)^3 \int \frac{x^4}{\left[\left(\frac{K^2 A x^2}{\hbar^2} + (B_1 + B_2)T\right)\right]} \times \frac{e^x}{(e^x - 1)^2} dx \tag{52}$$

According to (40), $\beta = (\hbar/KT)^3 I_2/I_3$, here

$$I_3 = B_2 T^3 \left(\frac{KT}{\hbar}\right)^2 \int_0^{\frac{\theta}{T}} \frac{A\omega^4 + B_1 T^3 \omega^2 + \frac{C}{L}}{\left[A\omega^4 + (B_1 + B_2)T^3\omega^2 + \frac{C}{L}\right]} \times \frac{x^6 e^x}{(e^x - 1)^2} dx, \tag{53}$$

We approximate this integral as follows:

$$I_3 = B_2 T^3 \left(\frac{KT}{\hbar}\right)^2 \int_0^{\propto} \frac{x^6 e^x}{(e^x - 1)^2} dx,$$

$$= \frac{16\pi^6}{21} B_2 T^3 \left(\frac{KT}{\hbar}\right)^2 \tag{54}$$

Now,

$$\beta = \frac{7}{164}\left(\frac{\hbar}{\pi KT}\right)^4 \left\{1 - \frac{3}{2\pi}\frac{\hbar}{K}\left[\frac{(B_1+B_2)T}{A}\right]^{\frac{1}{2}}\right\} \tag{55}$$

Then

$$\beta I_2 = \frac{7B_2\hbar^3}{48\pi^2 A^2 K^3}\left\{1 - \frac{3}{\pi}\frac{\hbar}{K}[\frac{(B_1 + B_2)T}{A}]^{1/2}\right\}.$$

This result can now be combined with (49) and (44) to obtain the total thermal conductivity.

$$K = \frac{K}{4\pi cT^{\frac{3}{2}}}\frac{1}{[A(B_1+B_2)]^{\frac{1}{2}}}\left[1-\frac{\left(\frac{cA}{L}\right)^{\frac{1}{2}}}{(B_1+B_2)T^3}\right]+\frac{7B_2\hbar^3}{96\pi^4K^2cA^2}\left\{1-\frac{3}{\pi}\frac{\hbar}{K}\left[\frac{(B_1+B_2)T}{A}\right]\right\}^{\frac{1}{2}} \quad (56)$$

The thermal conductivity of a large sample of material in the temperature region considered deviates from $T^{-3/2}$ by a correction roughly independent of temperature. We found,

$$I_2 = \frac{B_2}{(B_1+B_2)}\left(\frac{KT}{\hbar}\right)^3\int_0^{\propto}\frac{x^4e^x}{(e^x-1)^2}dx$$

$$= \frac{4\pi^4}{15}\frac{B_2}{(B_1+B_2)}\left(\frac{KT}{\hbar}\right)^3 \quad (57)$$

$$I_2 = \frac{B_1B_2T^3}{(B_1+B_2)}\left(\frac{KT}{\hbar}\right)^2\int\frac{x^6e^x}{(e^x-1)^2}dx$$

$$= \frac{16\pi^6}{21}\frac{B_1B_2T^3}{(B_1+B_2)}\left(\frac{KT}{\hbar}\right)^2 \quad (58)$$

Now,

$$\beta = 7\hbar^2/(20\pi^2K^2B_1T^5)$$

The thermal conductivity of the pure material is

$$\mathrm{K} = \frac{K^2}{6\hbar(B_1+B_2)cT^2}\left[1-\frac{3}{\pi^2}e^{-\frac{\theta}{T}}\left(\frac{\theta^2}{T^2}+\frac{2\theta}{T}+2\right)-\frac{3\hbar}{2\pi KT^{\frac{5}{2}}}\left[\frac{c}{L(B_1+B_2)}\right]^{\frac{1}{2}}+\frac{7}{25}\frac{B_2}{B_1}\right] \quad (59)$$

At very low temperatures, we found:

$$\beta = \frac{L}{c};\ \beta I_2 = \left(\frac{16\pi^6}{21}\right)B_2T^3\left(\frac{KT}{\hbar^5}\right)\left(\frac{L}{c}\right)^2 \quad (60)$$

After combining (60) with (48) in (44), that

$$K = \frac{2K\pi^2}{15}\frac{L}{c^2}\left(\frac{\pi KT}{\hbar}\right)^3\left[1-16A\left(\frac{\pi KT}{\hbar}\right)^4\frac{L}{c}-\frac{20}{7}B_1T^3\left(\frac{\pi KT}{\hbar}\right)^2\frac{L}{c}\right], \quad (61)$$

This way we can calculate thermal conductivity.

Chapter 5

5.0 Thermoelectric Device Basics:

Based on the thermoelectric effects that have been described earlier, we can build a thermoelectric module for power generation. Thermoelectric devices consist of many pairs of p-type and n-type semiconductors pellets. They are connected electrically in series and thermally in parallel. Taking one pellet working in the power generation mode, it can be solved for the temperature distribution along the leg when the two ends are subject to constant temperatures. Again, if we assume one-dimensional transport along the pellet axis with temperature-independent properties, we can also find the Thomson coefficient of zero, the equation can be solved readily for the temperature distribution. Applying Seebeck coefficient under open and an energy balance at the two boundaries, we find the heat transfer at the two boundaries is

$$Q_{H,P} = S_P I T_H - \frac{I^2 \rho_P L_P}{2A_P} + \frac{K_P A_P (T_H - T_C)}{L_P} \tag{62}$$

$$Q_{C,P} = S_P I T_C + \frac{I^2 \rho_P L_P}{2A_P} + \frac{K_P A_P (T_H - T_C)}{L_P} \tag{63}$$

Where ρ is the electrical resistivity, L is the length of leg and A is the cross-sectional area of the leg. The first term represents Peltier heat, the second term is due to Joule heating and the third term is due to heat conduction. The subscript p denotes properties of the p-type pellet.

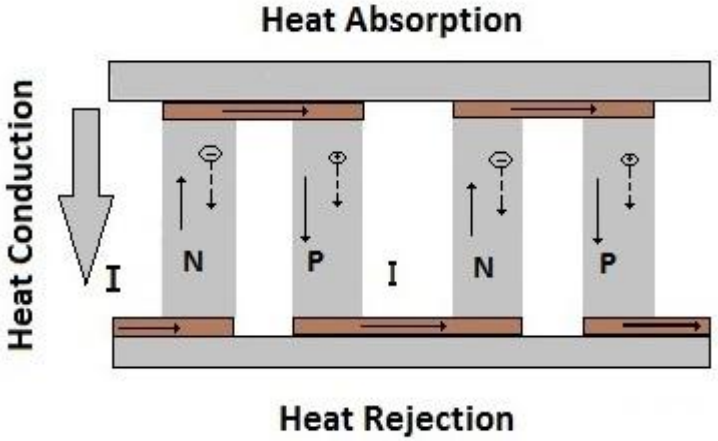

Figure 5(a). Thermoelectric module with many pairs of p-type and n-type semiconductor pellets connected electrically in series and thermally in parallel. (Replicated from [22])

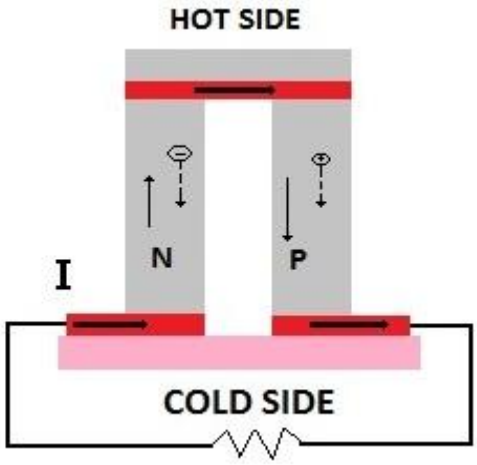

Figure 5(b). Schematic of thermoelectric power generator shown with one p-n pair.

(Replicated from [22])

For a power generation device with both n-type and p-type legs, the electrical resistance of the two legs in series is

$$R = \frac{L_P \rho_P}{A_P} + \frac{L_n \rho_n}{A_n} \tag{64}$$

And the thermal conductance of the two legs is

$$K = \frac{K_P A_P}{L_P} + \frac{K_n A_n}{L_n} \tag{65}$$

5.1 Progress in Thermoelectric Materials:

5.1.1 PGEC Materials:

Typical examples of PGEC thermoelectric materials are skutterudites, clathrates and b-Zn_4Sb_3. $CoSb_3$ is a typical skutterudites compound. The power factor of $CoSb_3$ is very high. However, its lattice thermal conductivity is too high to be an effective thermoelectric material. Void-filling in the structure with many different elements works as a successful approach to improve the figure of merit. The materials can be anything from lanthanide, actinide, alkaline-earth, alkali, and Group

IV elements [6]. The lattice thermal conductivity can be substantially reduced when these atoms acts as effective phonon scattering centers. Smaller and heavier atoms in the voids would result in larger disorder and lead to larger reduction of the lattice thermal conductivity on two branches of materials. Skutterudites [26-30] is one of them and other is clathrates [31-34] and β-Zn_4Sb_3 [35,36,37].

The clathrates are low-thermal conductivity compounds with open frame works composed of tetrahedral coordinate Si, Ge, Al, Ga, or Sn. The framework has cages that can incorporate large electro positive e atoms. There are two main types of structure, so-called Type Land Type II, with the former being more common.

Recent research for optimizing the thermoelectric properties of Type I clathrates above room temperature showed the best performance, as shown $Ba_8Ga_{16}Ge_{30}$ crystalline ingot showed a Seebeck coefficient of -45 to -150 mVK^{-1} and electrical conductivity 1500–600 Scm^{-1} at 300–900K. The thermal conductivity of this sample decreased from 1.8 $Wm^{-1}K^{-1}$ at 300K to 1.25 $Wm^{-1}K^{-1}$ at 900K, which gave rise to ZT of 1.35. In filled skutterudites [39-43] the values of ZT is greater than 1. A crystalline ingot $Ba_8Ga_{16}Ge_{30}$ showed a Seebeck coefficient at -45 to -150 mVK^{-1} and the electrical conductivity is between 600-1500 Scm^{-1} at 300-900K [44].

5.1.2 Nanostructured Materials:

Low-dimensional thermoelectric materials are believed to have higher thermoelectric properties than their bulk counterparts, because the DOS near Fermi level can be enhanced via quantum confinement therefore leading to the increase of thermo power; and/or because phonons over a large mean free path range can be effectively scattered by high density of interfaces, hence resulting in the decrease of the lattice thermal conductivity. Significant ZT enhancement has been found in

1. two-dimensional (2D) and
2. one- dimensional (1D) thermoelectric materials.

2D Thermoelectric nanomaterials:

The two dimensional Bi_2Te_3 quantum well had significant improvement in its ZT value due to Kicks and Dresselhaus [55] pioneering work. This happened due to the enhancement of thermos power because this will make a quantum confinement in the interlayer direction which can increase the DOS near the Fermi level. The highest ZT=2.4 was observed by Venkatasubramanian et al. [56] using Bi_2Te_3–Sb_2Te_3 quantum well superlattices. They had a periodicity of 6 nm. However, the highest ZT value for the bulk counterparts is only ZT=1.1. Knowing that quantum confinement may lead to an increased Seebeck coefficient and therefore higher ZT, Harman and coworkers [57] developed quantumdot superlattices in the PbTe–PbSeTe system. They were known as PbSe nanodots embedded in a PbTe matrix. It showed ZT=1.6, which is significantly higher than their bulk counterparts (ZT=0.34). Two-dimensional thin films and quantum well structures also showed enhanced thermoelectric properties. This includes Bi_2Te_3 superlattice-based thin-film [58], PbTe/Ag_2Te thin films [59], quantum well/ barrier PbTe/$Pb_{1-x}Eu_xTe$ structures [60], and n-PbTe/p-SnTe/n-PbTe quantum wells [61]. Shakouri [62] considered that sharp features in the electronic density of states of quantum-confined structures enable a doping-level-tunable increase in the asymmetry between hot and cold electron transport. This results in a large average transport energy and a large number of carriers moving in the [63]. Small heat loads or low levels of power generation are required in devices based on two-dimensional thermoelectric materials (such as thin film, quantum well, and super lattices) that may be used for small-scale electronic and optoelectronics applications [58].

1D Thermoelectric nanomaterials:

Due to additional electron confinement, then the theoretical studies predict a large enhancement in the value of the figure of merit inside the quantum wires. A greater enhancement in thermos-electric performance was suggested for the Quantum nanowires. This was due to their stronger quantum confinement and phonon scattering with respect to its two-dimensional counterparts [45]. Also there has been a proposal made that nanotubes may have a lower lattice thermal conductivity than the nanowires. The reason behind this is that there is additional phonon scattering on the inner and outer surfaces of nanotubes [46,47]. In one-dimensional materials, there have been many reports on the enhancement of thermoelectric properties. Hochbaum et al. reported that at room temperature for 50 nm diameter silicon nanowires a ZT of 0.6 can be obtained. This can be done

with rough surfaces synthesized by electrolysis etching, that represents a 60-times increase in ZT compared to its bulk counterpart. This happens because the rough nanowire surface could scatter phonons effectively [48]. As mentioned by, Boukai [19], the thermal conductivity decreases with decreasing the nanowire diameter. He reported a ZT of 1 at 200K for nanowires with 20 nm diameter. This resulting from the significant decrease of thermal conductivity and an enhanced phonon drag contribution to the thermos power. This is the first claim that phonon drag can enhance ZT significantly in rough nanowires. Transport of certain phonon modes can increase the Seebeck coefficient, which have minimal contribution to thermal conductivity [49]. Some nanowires have equal or lower thermoelectric properties compared to their bulk materials [50,51]. The limited ability to control dopant and impurity concentrations in nanowires can contribute to this [51,52]. This can also happen due to unintentional doping resulting from surface oxidation [53]. A potential module to assemble the thermoelectric device is made up of a p–n heterostructure. Ensuring good electrical contact to all nanowires in the array, minimizing matrix heat leakage is preventing measuring any significant enhancement in nanowire composites and having high packing densities is the main challenge here [54].

5.1.3 Nano-Composite Materials:

By increasing the phonon scattering Nano-composite bulk materials can reduce the lattice thermal conductivity. As the phonon mfp typically ranges from several nanometers up to a few hundred nanometers, preferential phonon scattering is possible. This is because the carrier mfp is typically only a few nanometers [64]. For this reason, incorporating a nanostructures covering various length scales can reduce the lifetime of phonons with a broad mfp distribution. However, charge transport can remain unchanged [64]. Nano structuring composites are made through the formation of nanometer-sized polycrystalline. This is typically fabricated by hot pressing or spark plasma sintering of fine powders. The powders are formed by grinding and milling or wet chemistry processing. In this process thermoelectric materials are prepared in Nano sized particles and are then hot pressed into monoliths. To provide the large volume of material necessary for more wide-spread adoption of thermoelectric technology compacting nanocrystal- line samples can be a relatively low-cost method. ZT enhancement has been found in the many kinds of nanostructured

material families. They include Bi_2Te_3-based nanocomposites, PbTe-based nanostructured materials and SiGe-based nanocomposites.

5.2 Calculating Electrical Performance in Thermoelectric Generator:

The direct conversion of temperature differences to electric voltage or the other way around is called the thermoelectric effect. Devices such as thermoelectric coolers for electronic cooling or portable refrigerators work on this mechanism. Though, Joule heating is an irreversible phenomenon, the thermoelectric effect is reversible. The thermoelectric effect is known under three different names. The reason behind it is that it was discovered during experiments by Seebeck, Peltier, and Thomson. The Seebeck effect is the conversion of temperature differences into electricity, the Peltier effect is the conversion of electricity to temperature differences, while the Thomson effect is heat produced by the product of current density and temperature gradients.

These Seebeck, Peltier and Thomson effects are thermodynamically related by the Thomson relations:

$$P = ST \tag{65}$$

$$\mu = T\frac{dS}{dT} \tag{66}$$

where P is the Peltier coefficient (SI unit: V), S is the Seebeck coefficient (SI unit: V/K), T is the temperature (SI unit: K), and μ is the Thomson coefficient (SI unit: V/K). These relations show that all three effects can be considered as one and the same effect. This example primarily uses the Seebeck coefficient and also the Peltier coefficient. The Thomson coefficient is not used. The flux quantities of interest when simulating the thermoelectric effect are the heat flux q and the flux of electric current J:

$$q = -kT\nabla + PJ \tag{67}$$

$$J = -\sigma\nabla V - \sigma S\nabla T \tag{68}$$

Some other quantities of relevance are:

$$E = -\nabla V \tag{69}$$

$$Q = JE \tag{70}$$

where E is the electric field and Q is the Joule heating. Conservation of heat energy and current gives:

$$\rho C \frac{\partial T}{\partial t} + \nabla . q = Q \tag{71}$$

$$\nabla . J = - \frac{\partial \rho C}{\partial T} \tag{72}$$

where ρ is the density, *C* is the heat capacity, and ρc is the space charge density. In this example, consider the stationary case only:

$$\nabla . q = Q \tag{73}$$

$$\nabla . J = 0 \tag{74}$$

More explicitly, the thermoelectric equations become:

$$\nabla . \left(-kT\nabla + P(-\sigma\nabla V - \sigma ST\nabla)\right) = (-\sigma\nabla V - \sigma ST\nabla).(-\nabla V)\nabla\sigma.(-\nabla V - \sigma ST\nabla) = 0 \tag{75}$$

It is difficult to work with the explicit form of the equations. This example makes use of a series of intermediate variables to simplify them.

The partial differential equations are required to be entered in the weak form. To transfer to weak form, multiply each of the two equations with the test functions corresponding to the unknowns' T and V (here called V_T and V_V, respectively) and integrate over the whole computational domain D:

$$\int_D (\nabla . \boldsymbol{q}) V_T = \int_D Q V_T \tag{76}$$

$$\int_D (\nabla . \boldsymbol{J}) V_V = 0 \tag{77}$$

Partial integration gives:

$$-\int_D \boldsymbol{q}.\nabla V_T + \int_B n.qV_T = \int_B QV_T \tag{78}$$

$$-\int_D J.\nabla V_V + \int_B n.JV_V = 0 \tag{79}$$

where B is the boundary of D, and n is the unit normal of D. Assuming that there are known values for the heat and current flux in the direction of the boundary normal as q0 and J0, respectively, the equations become:

$$-\int_D \boldsymbol{q}.\nabla V_T + \int_B q_0 V_T = \int_D QV_T \tag{80}$$

$$-\int_D J.\nabla V_V + \int_B J_0 V_V = 0 \tag{81}$$

It is required to enter the domain parts of the weak form equations while the boundary parts are more or less automatically available. The integrands of the domain parts are:

$$0 = q\nabla\, vT + QvT \tag{82}$$

$$0 = J\nabla.V_V \tag{83}$$

In addition to the domain weak form equations, a number of different boundary conditions are implemented:

$$T = T_0$$

$$V = V_0$$

$$\mathrm{q}_0 = 0$$

$$J_0 = 0$$

$$\mathrm{q}_0 = \mathrm{q}_{in}$$

- The first condition sets a temperature T_0 on a boundary.
- The second condition sets a voltage V_0 on a boundary.

- The natural boundary conditions set the heat flux and current density on the boundary to zero. They arrive "naturally" as part of the weak form partial integration so they are called natural. The thermal and electrical insulation are represented by the natural boundary conditions. It is even necessary to define this bundled boundary condition because that would anyway have been available because any boundaries not explicitly set to a certain condition automatically obey the natural conditions. However, the natural boundary condition is available for better usability of the thermoelectric physics interface. As a result, we can clearly see which boundaries are insulated.

- The last boundary condition sets the value of the heat flux in the direction of the boundary normal. The heat flux boundary condition is implemented with a weak equation which is one of the terms in the complete weak form equation for the heat transfer part of the thermoelectric equations, as seen earlier.

$$\int_B \mathrm{q}_0 V_T$$

which is one of the terms in the complete weak form equation for the heat transfer part of the thermoelectric equations, as seen earlier.

Chapter 6

6. Design and Analysis

6.1 Material Design and Analysis:

Here, we will discuss about the design and analysis steps of our report. First of all, we have chosen different materials to study on and found out the values of the Thermal conductivity(K), Electrical conductivity (σ), Seebeck co-efficient(S) and Peltier co-efficient (Π) etc. From these values we have calculated the values of the thermoelectric figure of merit (ZT).

By utilizing these values, we have analyzed the TEG model to find out the electrical performance such as the Electrical potential(V) and Current density(J).

Si-n Type:

The figure (6) below shows that a negatively doped Silicon lattice nanostructure which is doped by a Phosphorous(P) atom which is positioned at Cartesian values (0.48×10^{-9},0.498×10^{-9}, 0.744×10^{-9}). The lattice structure has the measurements of length 1.646 nm, Width 0.576 nm and Depth 0.443nm.

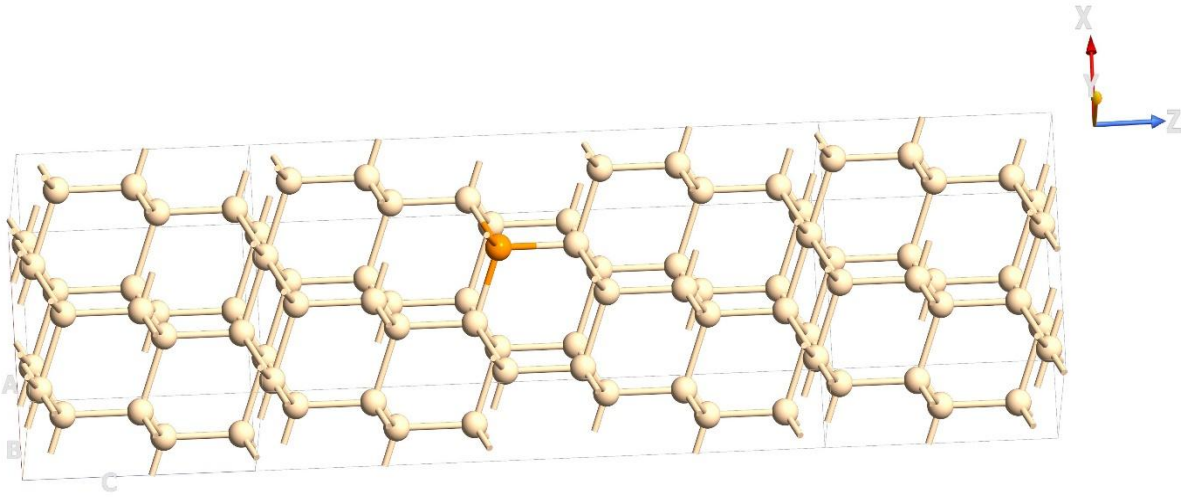

Figure 6. Si-n Type Lattice Nano Structure

At 310K, the values that we have obtained for this structure are K=495.26×10^{-3}W/Km, $\sigma = 425.367 \times 10^{3}$S/m, S=$-5.22\times 10^{-6}$ V/K , Π= -0.001566V and ZT=2.405.

At 305K, the values that we have obtained for this structure are K=486.15×10^{-3}W/Km, $\sigma = 426.593 \times 10^{3}$S/m, S=$-3.829\times 10^{-6}$V/K, $\Pi = -0.001168$V and ZT=2.3687.

At 300K, the values that we have obtained for this structure are K=467.79×10^{-3} W/Km, $\sigma = 427.883 \times 10^{3}$S/m, S=$-2.461\times 10^{-6}$V/K, $\Pi = -0.000763$V and ZT=2.334.

Table 3. Si- n Type Electronic Properties

Materials Name	Temperature (K)	Thermal Conductivity (W/Km)	Electric Conductivity (S/m)	Seebeck Coefficient (V/K)	Peltier Coefficient (V)	Figure of Merit ZT
Si-n Type	310	495.26×10^{-3}	425.367×10^{3}	-5.22×10^{-6}	-0.001566	2.405
	305	486.15×10^{-3}	426.593×10^{3}	-3.829×10^{-6}	-0.001168	2.3687
	300	467.79×10^{-3}	427.883×10^{3}	-2.461×10^{-6}	-0.000763	2.334

Si-P Type:

The figure (7) below shows that a positively doped Silicon lattice nanostructure which is doped by an Aluminum(Al) atom which is positioned at Cartesian values (0.469×10^{-9},0.278×10^{-9}, 1.06×10^{-9}). The lattice structure has the measurements of length 1.645 nm, Width 0.574 nm and Depth 0.554nm.

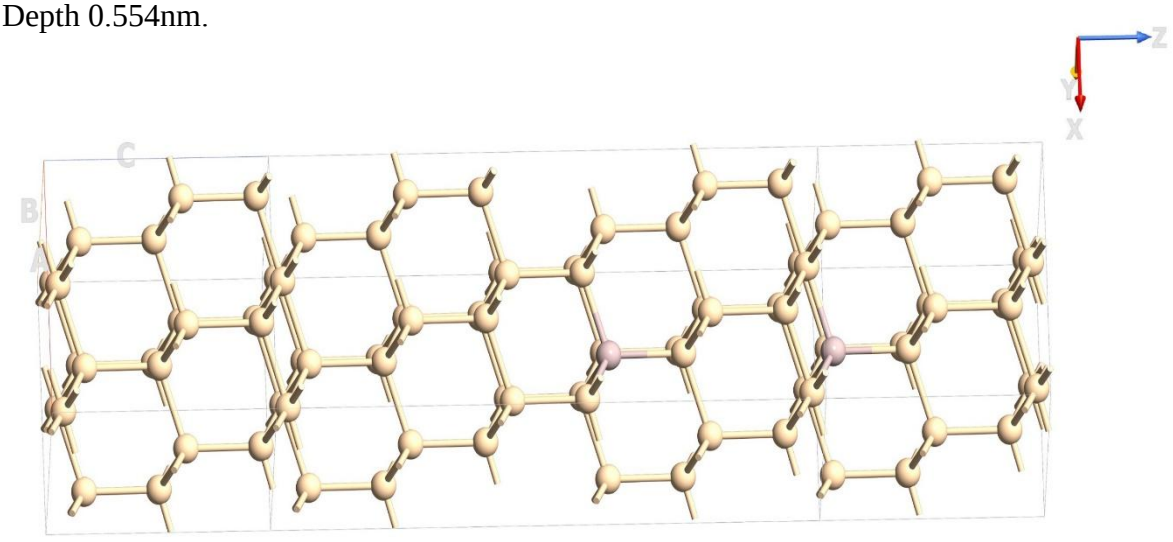

Figure7. Si-p Type Lattice Nano Structure

At 300K, the values that we have obtained for this structure are K=204.924× 10^{-3} W/Km, $\sigma = 354.936 \times 10^{3}$S/m, S=6.197× 10^{-5} V/K , Π= 0.01859V and ZT=2.8500.

At 305K, the values that we have obtained for this structure are K=201.581× 10^{-3}W/Km, $\sigma = 352.404 \times 10^{3}$S/m, S=6.259× 10^{-5}V/K, $\Pi = 0.01909$V and ZT=2.795.

At 310K, the values that we have obtained for this structure are K=198.176× 10^{-3}W/Km, $\sigma = 349.924 \times 10^{3}$S/m, S=6.318× 10^{-5}V/K, $\Pi = 0.1959$V and ZT=2.742.

Table 4. Si- p Type Electronic Properties

Materials Name	Temperature (K)	Thermal Conductivity (W/Km)	Electric Conductivity (S/m)	Seebeck Coefficient (V/K)	Peltier Coefficient (V)	Figure of Merit ZT
Si-p Type	300	204.924× 10^{-3}	354.936× 10^{3}	6.197× 10^{-5}	0.01859	2.850
	305	201.581× 10^{-3}	352.404× 10^{3}	6.259× 10^{-5}	0.01909	2.795
	310	198.176× 10^{-3}	349.924× 10^{3}	6.318× 10^{-5}	0.1959	2.742

SiGe:

From the figure (8) below shows that a Silicon-Germanium lattice. The lattice structure has the measurements of length 2.636 nm, Width 1.108 nm and Depth 0.576nm.

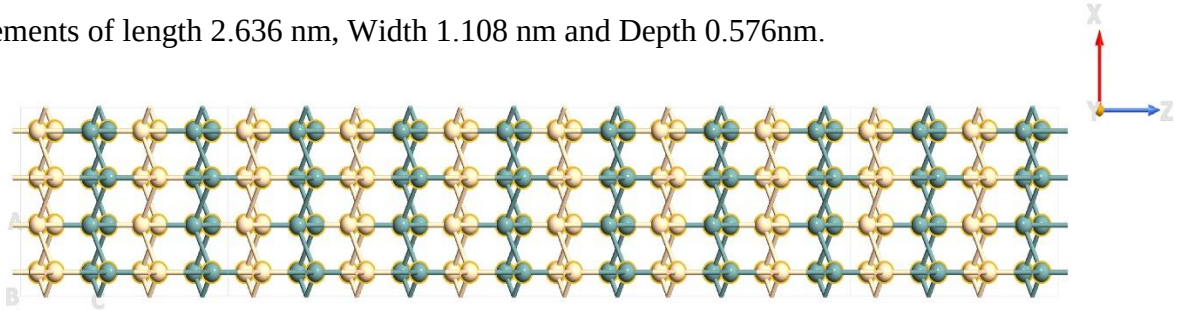

Figure 8. SiGe Lattice Nano Structure

At 300K, the values that we have obtained for this structure are K=3.455 W/Km, $\sigma = 557.186 \times 10^3 \mathrm{S/m}$, S=5.994$\times 10^{-8}$ V/K , Π=1.789$\times 10^{-5}$V and ZT=2.320.

At 305K, the values that we have obtained for this structure are K=3.508 W/Km, $\sigma = 556.773 \times 10^3 \mathrm{S/m}$, S=1.368$\times 10^{-7}$V/K, $\Pi = 4.175 \times 10^{-5}$V and ZT=2.304.

At 310K, the values that we have obtained for this structure are K=3.561 W/Km, $\sigma = 555.95 \times 10^3 \mathrm{S/m}$, S=2.125$\times 10^{-7}$V/K, $\Pi = 6.586 \times 10^{-5}$V and ZT=2.28.

Table 5. SiGe Electronic properties

Materials Name	Temperature (K)	Thermal Conductivity (W/Km)	Electric Conductivity (S/m)	Seebeck Coefficient (V/K)	Peltier Coefficient (V)	Figure of Merit ZT
SiGe	300	3.561	557.186×10^3	5.994×10^{-8}	1.789×10^{-5}	2.320
	305	3.508	556.773×10^3	1.368×10^{-7}	4.175×10^{-5}	2.304
	310	3.455	555.95×10^3	2.125×10^{-7}	6.586×10^{-5}	2.28

MoS2:

We can see from the figure (9) below shows that a Molybdenite-Disulphide lattice. The lattice structure has the measurements of length 1.145 nm, Width 0.945nm and Depth 0.799 nm.

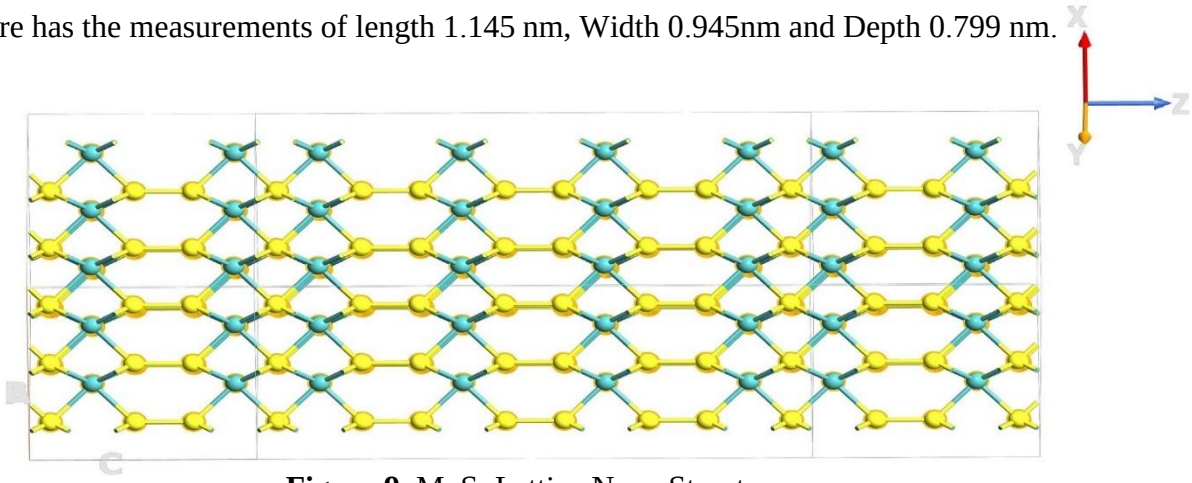

Figure 9. MoS_2 Lattice Nano Structure

At 300K, the values that we have obtained for this structure are K=44.757× 10^{-3}W/Km, $\sigma = 35.873 \times 10^{3}$S/m, S=8.315× 10^{-5}V/K , Π=0.02494V and ZT=4.39229.

At 305K, the values that we have obtained for this structure are K=45.631× 10^{-3}W/Km, $\sigma = 36.149 \times 10^{3}$S/m, S=8.247× 10^{-5}V/K, $\Pi = 0.02515$V and ZT=4.30173.

At 310K, the values that we have obtained for this structure are K=46.51× 10^{-3}W/Km, $\sigma = 36.421 \times 10^{3}$S/m, S=8.181× 10^{-5}V/K, $\Pi = 0.02536$V and ZT=4.216.

Table 6. MoS_2 Electronic Properties

Materials Name	Temperature (K)	Thermal Conductivity (W/Km)	Electric Conductivity (S/m)	Seebeck Coefficient (V/K)	Peltier Coefficient (V)	Figure of Merit ZT
	300	**44.757× 10^{-3}**	**35.873× 10^{3}**	**8.315× 10^{-5}**	**0.02494**	**4.39229**
MoS2	**305**	**45.631× 10^{-3}**	**36.149× 10^{3}**	**8.247× 10^{-5}**	**0.02515**	**4.30173**
	310	**46.51× 10^{-3}**	**36.421× 10^{3}**	**8.181× 10^{-5}**	**0.02536**	**4.216**

ZnO:

From the figure (10) below shows that a Zinc-Oxide lattice. The lattice structure has the measurements of length 1.145 nm, Width 0.945nm and Depth 0.799 nm.

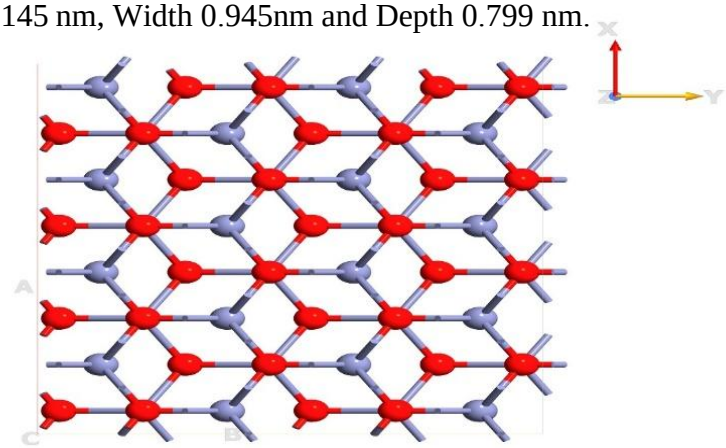

Figure 10. ZnO Lattice Nano Structure

Table 7. ZnO Electronic Properties

Materials Name	Temperature (K)	Thermal Conductivity (W/Km)	Electric Conductivity (S/m)	Seebeck Coefficient (V/K)	Peltier Coefficient (V)	Figure of Merit ZT
ZnO	300	20.393×10^{-3}	4.631×10^{3}	-4.594×10^{-5}	-0.01378	1.7072
	305	20.865×10^{-3}	4.635×10^{3}	-4.62×10^{-5}	-0.01409	1.7106
	310	21.354×10^{-3}	4.640×10^{3}	-4.643×10^{-5}	-0.01439	1.7108

At 300K, the values that we have obtained for this structure are K=20.393×10^{-3}W/Km, $\sigma = 4.631 \times 10^{3}$S/m, S=$-4.594\times 10^{-5}$V/K , Π=-0.01378V and ZT=1.7072.

At 305K, the values that we have obtained for this structure are K=20.865×10^{-3}W/Km, $\sigma = 4.635 \times 10^{3}$S/m, S=$-4.62\times 10^{-5}$V/K, $\Pi = -0.01409$and ZT=1.7106.

At 310K, the values that we have obtained for this structure are K=21.354×10^{-3}W/Km, $\sigma = 4.640 \times 10^{3}$ S/m, S=-4.643×10^{-5}V/K, $\Pi = -0.01439$V and ZT=1.7108.

6.2 TEG Design and Analysis:

For the device analysis we will use the one leg and two leg TEG module. The TEG structures will be novel modules. Its analysis consists of measuring the potential created across the two legs of the thermoelectric generator when a temperature difference is applied on both sides of it. We will also measure the current density at the surface of the legs to determine the amount of current that can be produced per unit area using this generator.

TEG based on Si-n Type (300K):

From figure (11) we can see the one-legged thermoelectric generator which consists of a Silicon-n-Type leg. The contact on the TEG was made of Copper. We will test the module at 300K. The

objective is to measure the potential across the one leg of the generator and also the surface current that it can produce. We will also look at the direction of current flow. From the figure (11), we can see that the highest electric potential is at $37.5 \times 10^{-3} V$. From the figure (11), we can also see that the current density is at $1.613 \times 10^{11} Am^{-2}$.

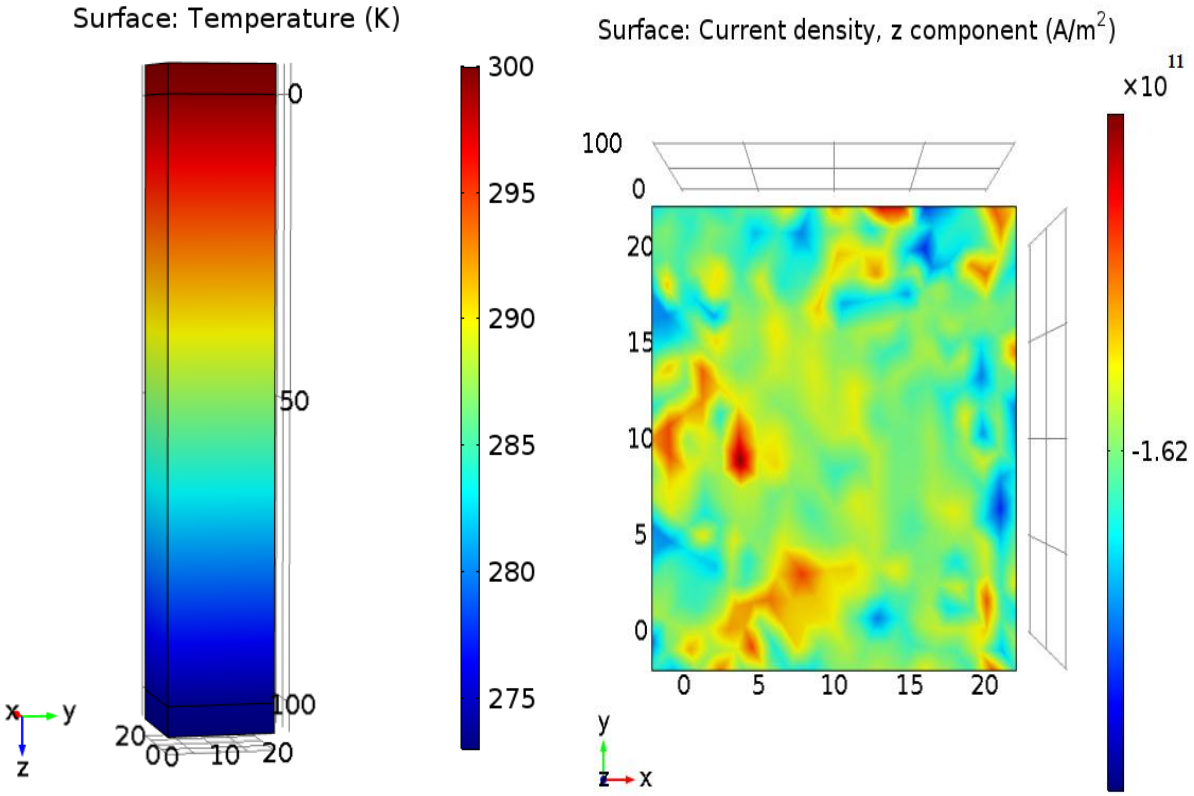

(a) (b)

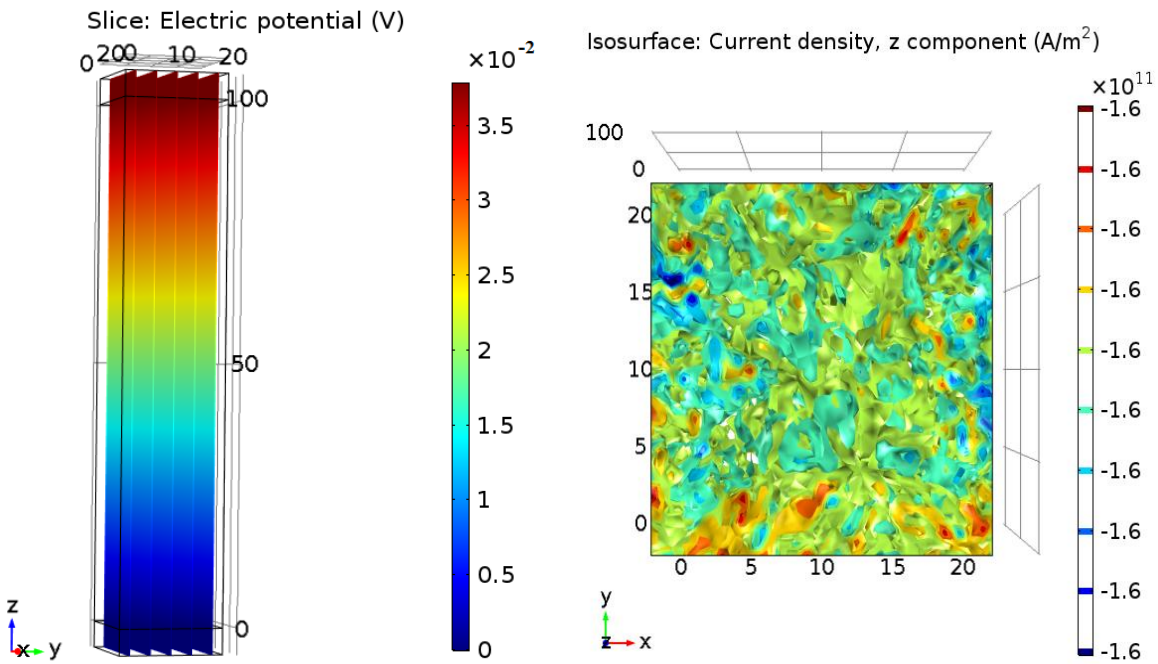

(c) (d)

Figure 11. (a)Temperature of Si-n-Type (b)Current Density of Si-n-Type using surface area. (c)Electric Potential using slice(d)Current Density of Si-n-Type using Isosurface at 300K

TEG based on Si-n Type (305K):

From figure (12) we can see the one-legged thermoelectric generator which consists of a Silicon-n-Type leg. The contact on the TEG was made of Copper. We will test the module at 305K. The objective is to measure the potential across the one leg of the generator and also the surface current that it can produce. We will also look at the direction of current flow. From the figure (12), we can see that the highest electric potential is $37.9 \times 10^{-3} V$. From the figure (12), we can also see that the current density is at $1.625 \times 10^{11} Am^{-2}$.

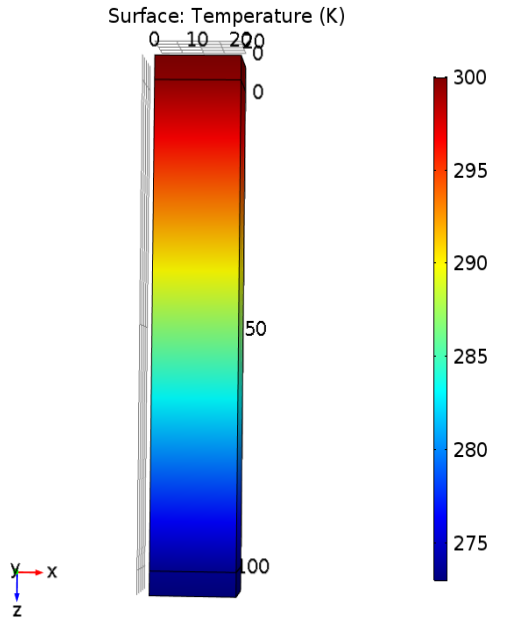

(a).

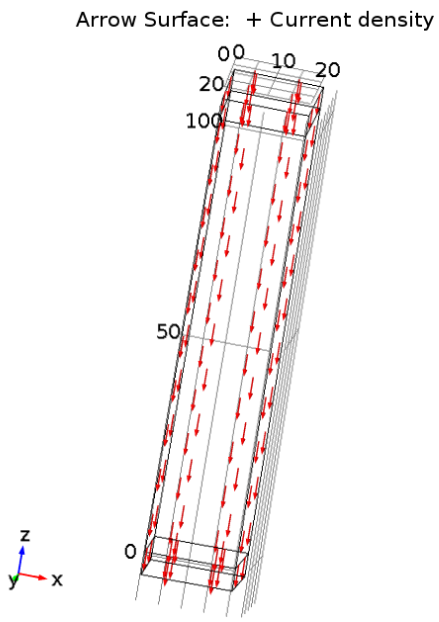

(b)

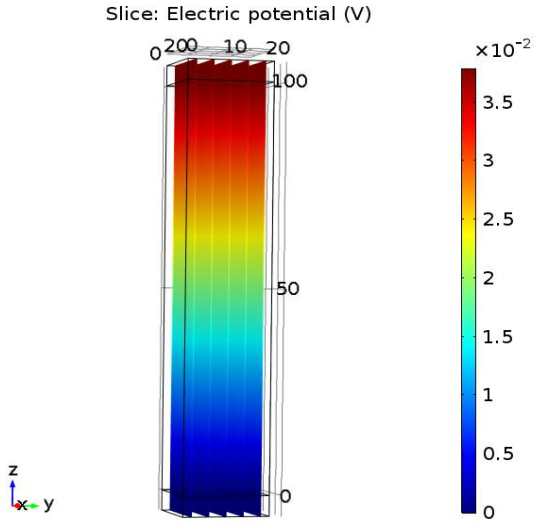

(c)

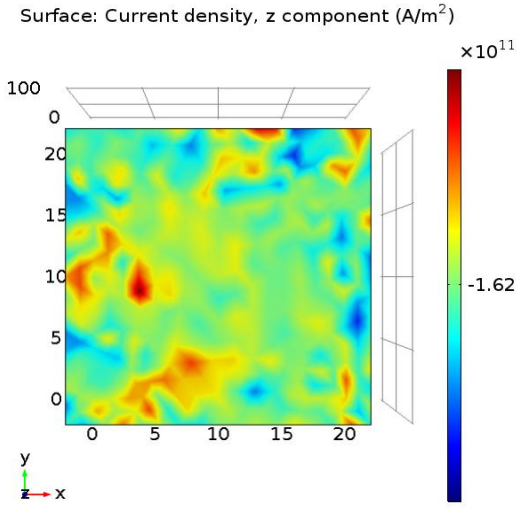

(d)

Figure 12. (a)Temperature of Si-n-Type (b) Current Density of Si-n-Type using arrow line. (c) Electric Potential (d) Current Density of Si-n-Type using surface area at 305K

TEG based on Si-n Type (310K):

From figure (13) we can see the one-legged thermoelectric generator which consists of a Silicon-n-Type leg. The contact on the TEG was made of Copper.

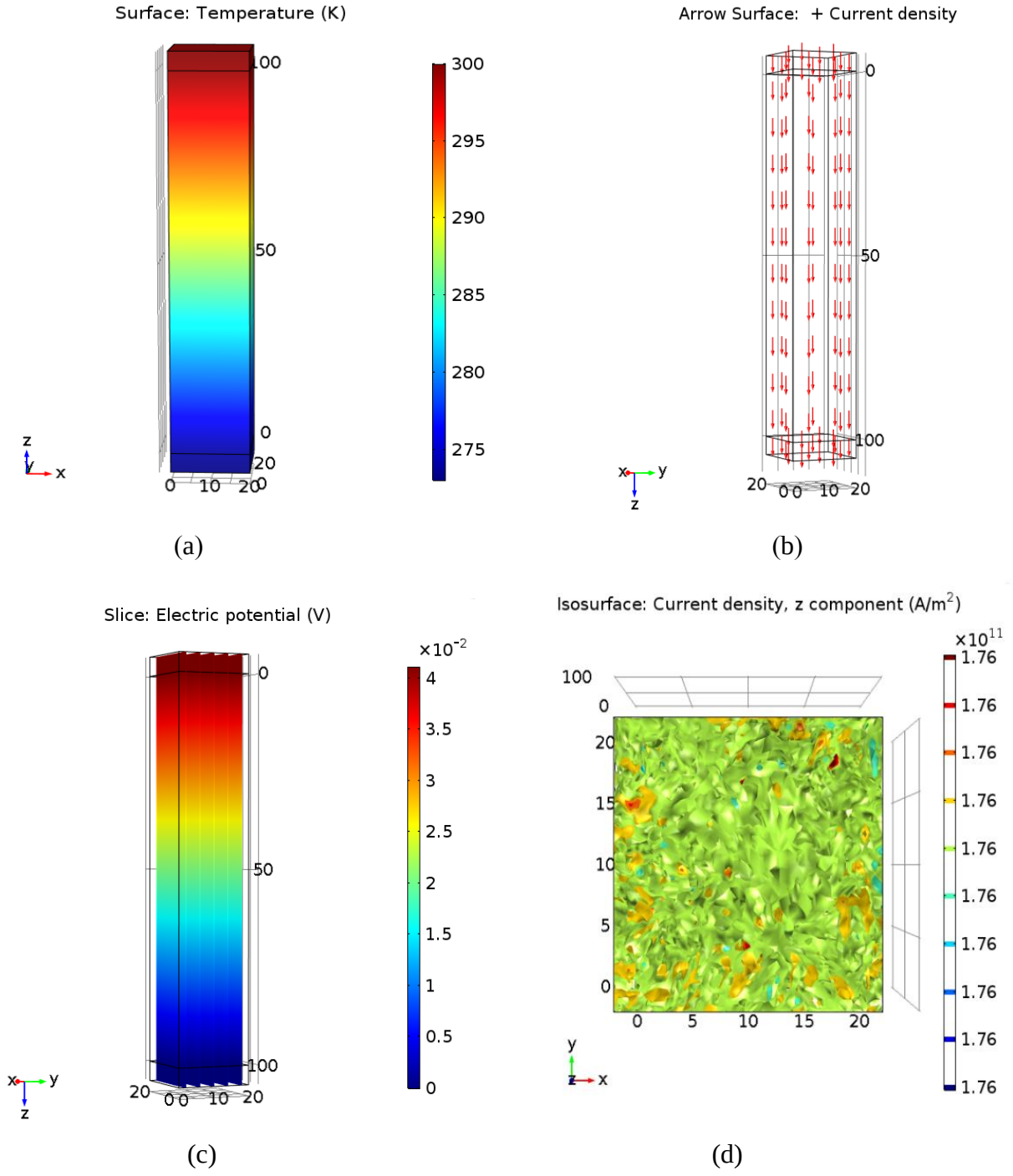

Figure 13. (a)Temperature of Si-n-Type (b) Current Density of Si-n-Type using arrow line (c) Electric Potential using slice(d) Current Density of Si-n-Type using Isosurface at 310K

We will test the module at 310K. The objective is to measure the potential across the one leg of the generator and also the surface current that it can produce. We will also look at the direction of current flow. From the figure (13), we can see that the highest electric potential is $41.1 \times 10^{-3}V$. From the figure (13), we can also see that the current density is at $1.632 \times 10^{11}Am^{-2}$.

TEG based on Si-n Type and SiGe(300K):

From figure (14) we can see the two-legged thermoelectric generator which consists of a Silicon-n-Type leg and also a SiGe leg. The contact on the TEG was made of Copper. The main objective of this study is to measure the potential across the two legs of the generator and also the surface current that it can produce. We will also look at the direction of current flow. From the figure (14), we can see that the highest electric potential is $55.63 \times 10^{-3}V$. From the figure (14), we can also see that the current density is at $1.21 \times 10^{11}Am^{-2}$.

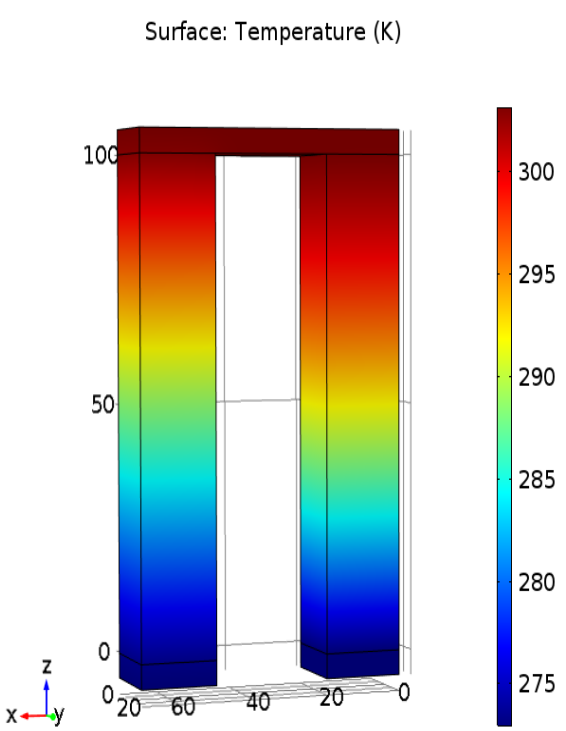

(a)

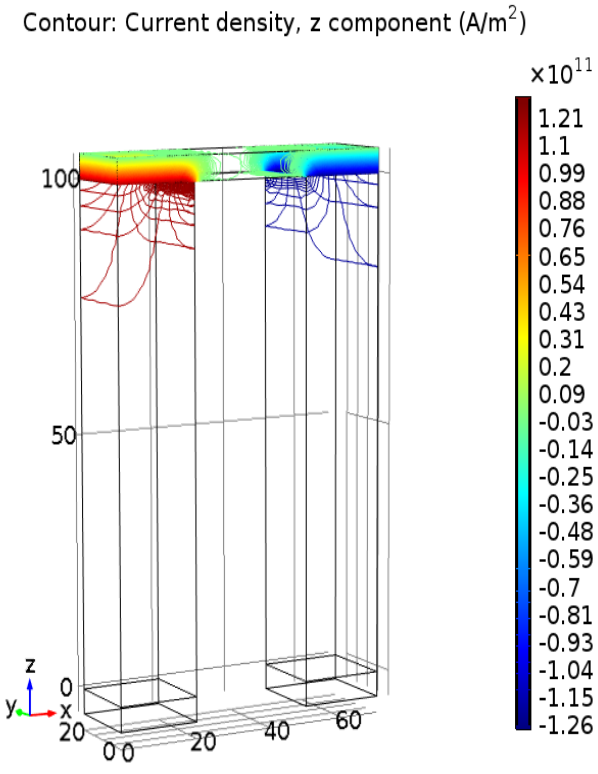

(b)

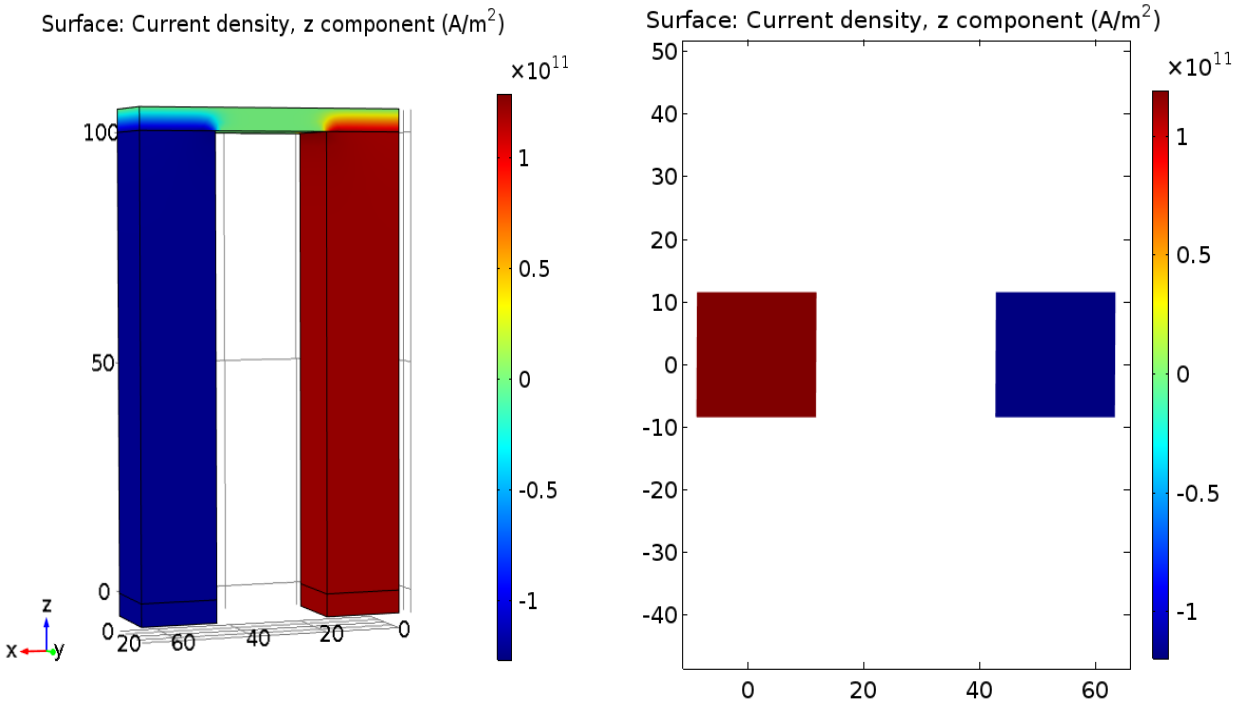

(c) (d)

Figure 14. (a)Temperature of Si-n Type and SiGe (b) Current Density of Si-n Type and SiGe using Contour. (c) Current Density of Si-n Type and SiGe using surface area (d) Current Density of Si-n Type using surface at 300K

TEG based on Si-n Type and SiGe(305K):

From figure (15) we can see the two-legged thermoelectric generator which consists of a Silicon-n-Type leg and also a SiGe leg. The contact on the TEG was made of Copper. The main objective of this study is to measure the potential across the two legs of the generator and also the surface current that it can produce. We will also look at the direction of current flow. From the figure (15), we can see that the highest electric potential is $58.92 \times 10^{-3} V$. From the figure (15), we can also see that the current density is at $1.28 \times 10^{10} Am^{-2}$.

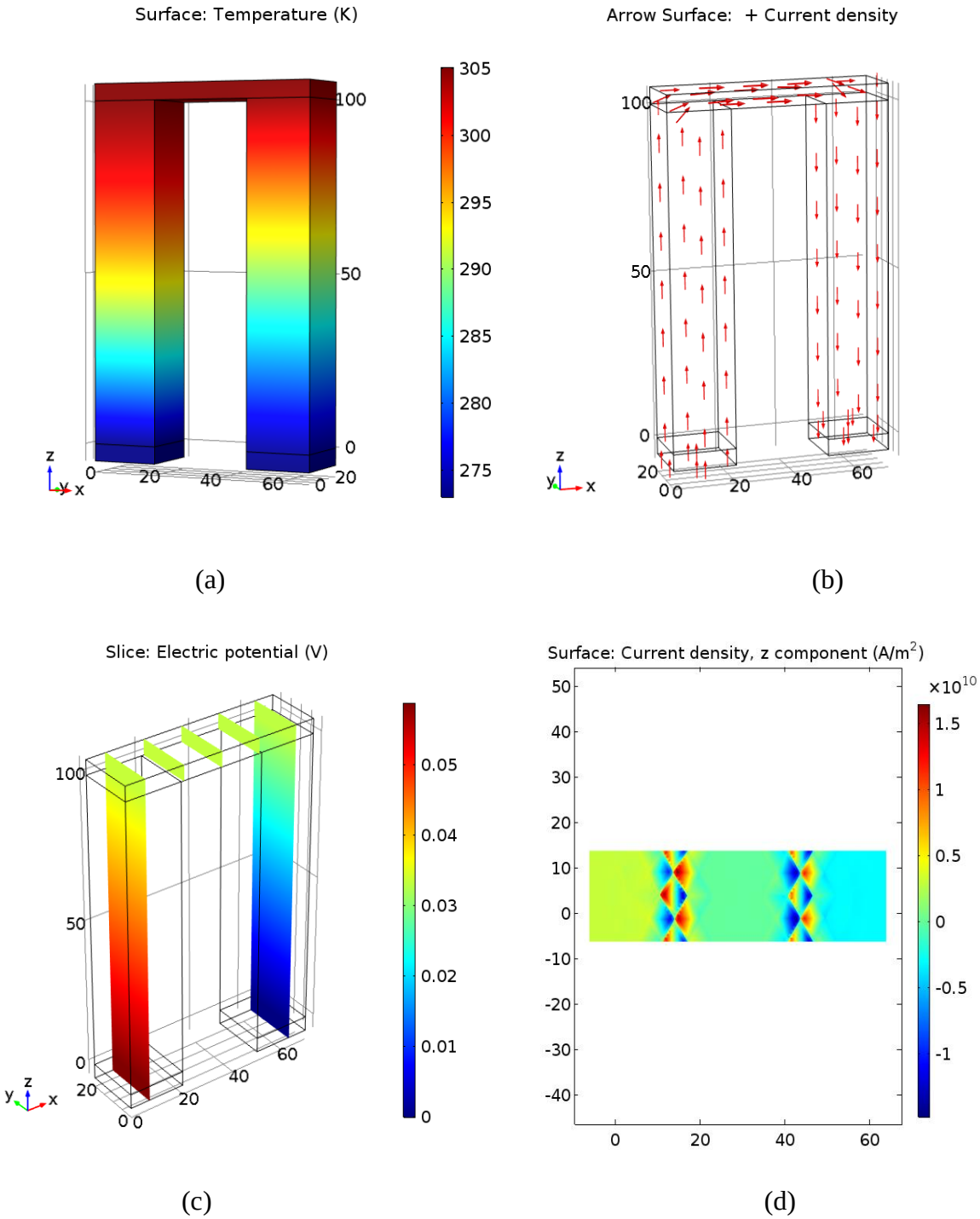

Figure 15. (a)Temperature of Si-n Type and SiGe (b) Current Density of Si-n Type and SiGe using arrow line. (c) Electric potential using slice. (d) Current Density of Si-n Type using surface at 305K

TEG based on Si-n Type and SiGe(310K):

From figure (16) we can see the two-legged thermoelectric generator which consists of a Silicon-n-Type leg and also a SiGe leg.

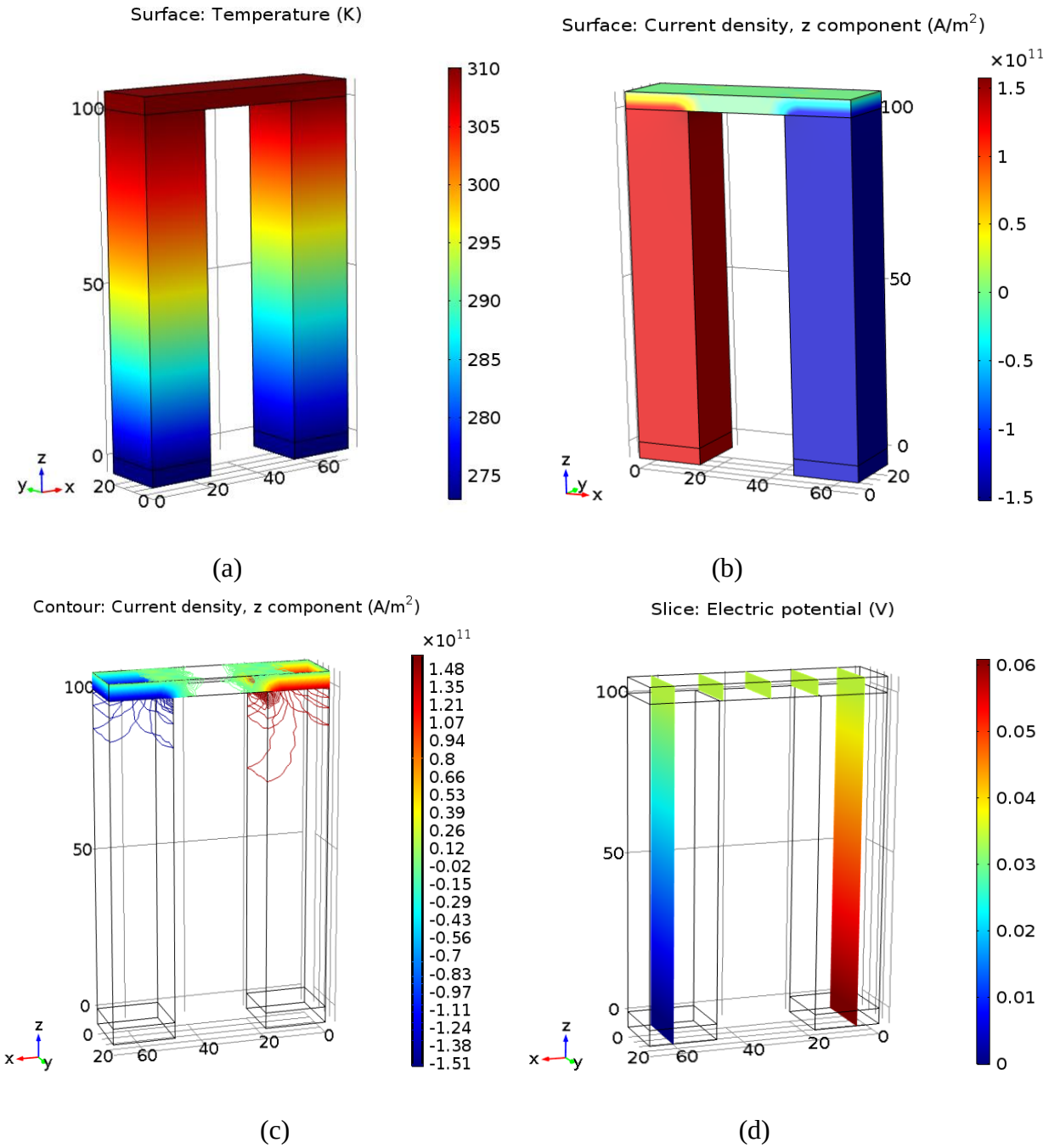

Figure 16. (a)Temperature of Si-n-Type and SiGe (b) Current Density of Si-n-Type and SiGe using surface area. (c) Current Density of Si-n-Type and SiGe using Coutour (d) Electric potential using slice at 310K

The contact on the TEG was made of Copper. The main objective of this study is to measure the potential across the two legs of the generator and also the surface current that it can produce. We will also look at the direction of current flow. From the figure (16), we can see that the highest electric potential is $65.01 \times 10^{-3}V$. From the figure (16), we can also see that the current density is at $1.31 \times 10^{11}Am^{-2}$.

TEG based on MoS_2 and ZnO (300K):

From figure (17) we can see the two-legged thermoelectric generator which consists of a MoS_2 and ZnO at 300K. The contact on the TEG was made of Copper. The main objective of this study is to measure the potential across the two legs of the generator and also the surface current that it can produce. We will also look at the direction of current flow. From the figure (17), we can see that the highest electric potential is $75.64 \times 10^{-3}V$. From the figure (17), we can also see that the current density is at $2.7 \times 10^{9}Am^{-2}$.

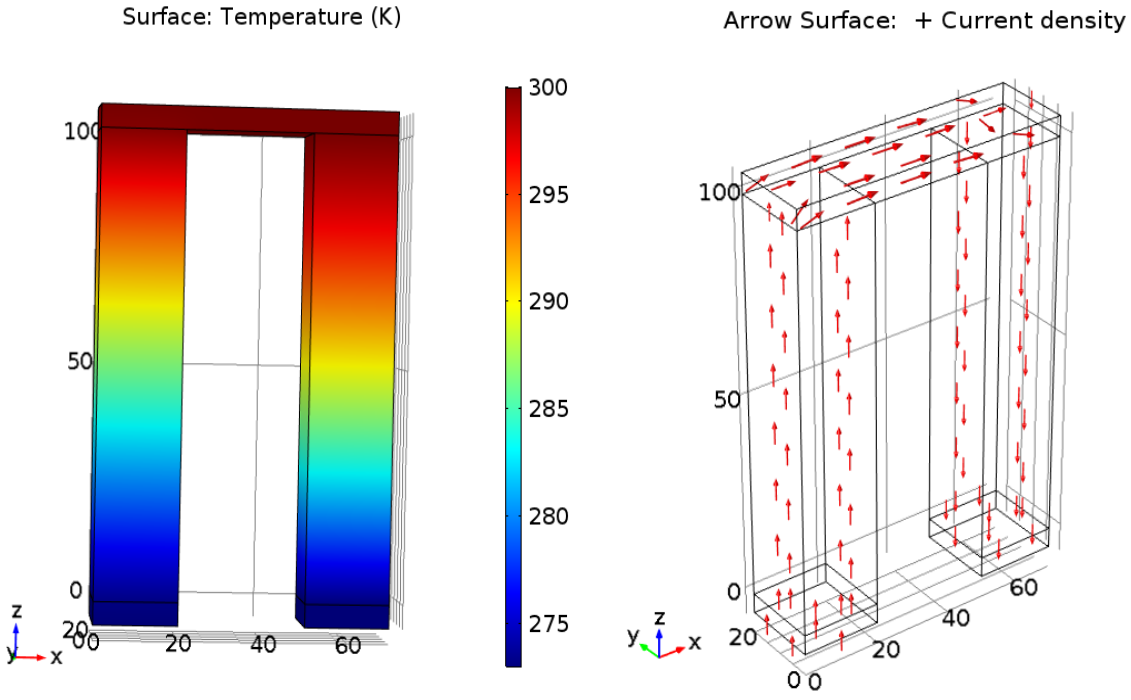

(a) (b)

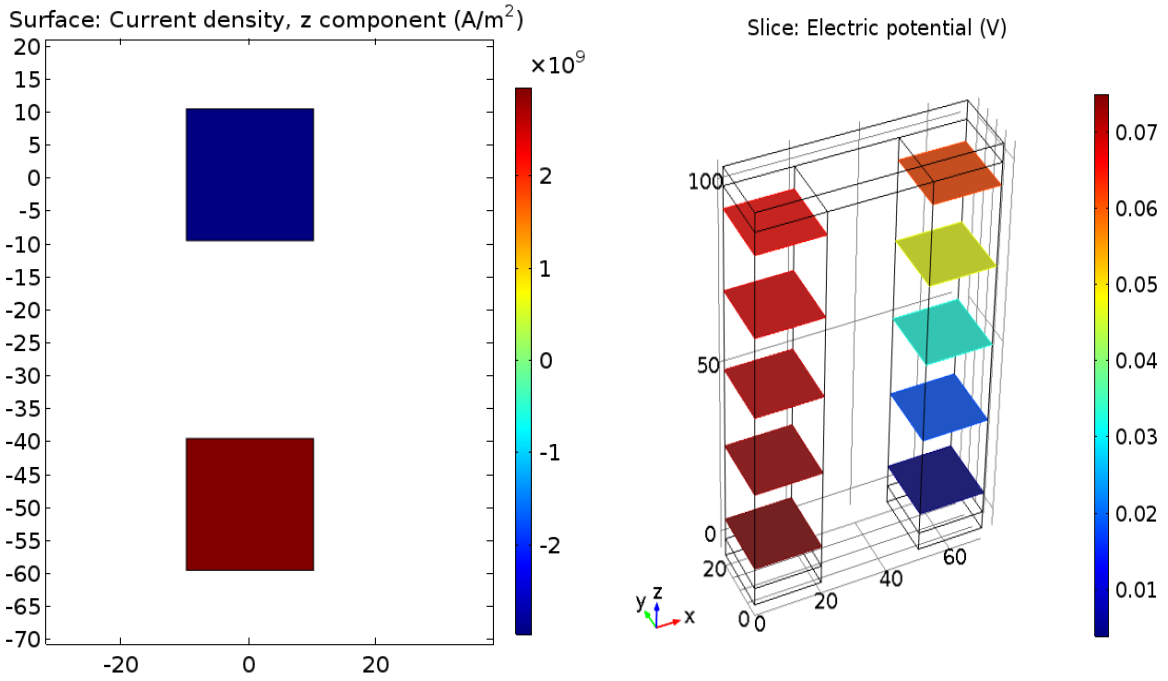

(c) (d)

Figure 17. (a)Temperature of MoS_2 and ZnO (b) Current Density of MoS_2 and ZnO using arrow line (c) Current Density MoS_2 and ZnO using surface (d) Electric potential using Slice at 300K.

TEG based on MoS_2 and ZnO (305K):

From figure (18) we can see the two-legged thermoelectric generator which consists of a MoS_2 and ZnO leg at 305K. The contact on the TEG was made of Copper. The main objective of this study is to measure the potential across the two legs of the generator and also the surface current that it can produce. We will also look at the direction of current flow. From the figure (18), we can see that the highest electric potential is $75.89 \times 10^{-3}V$. From the figure (18), we can also see that the current density is at $2.73 \times 10^{9}Am^{-2}$.

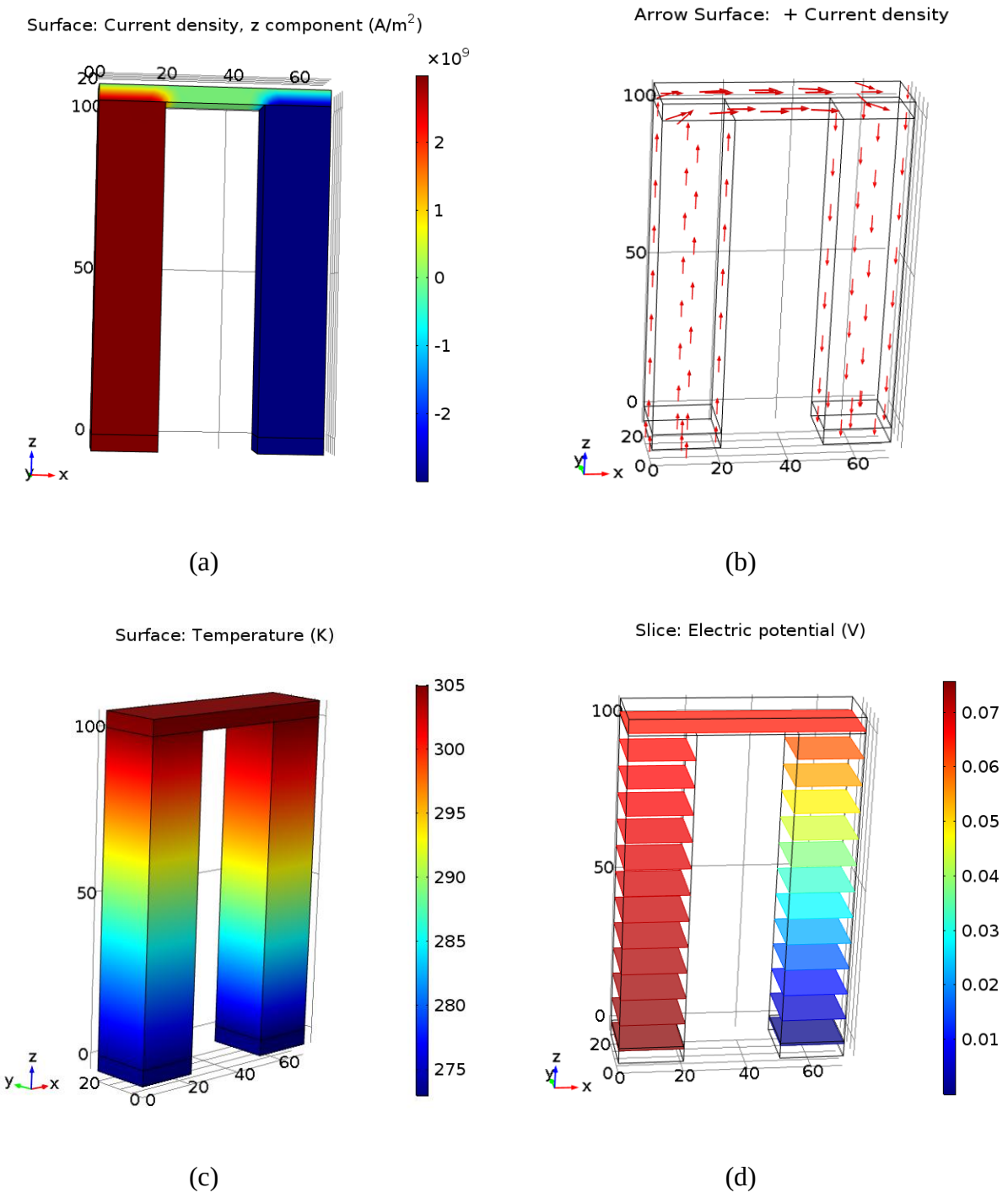

(a) (b)

(c) (d)

Figure 18. (a) Current Density of MoS_2 and ZnO using arrow line (b) Current Density of MoS_2 and ZnO using surface area. (c) Temperature MoS_2 and ZnO (d) Electric potential using Slice.

TEG based on MoS_2 and ZnO (310K):

From figure (19) we can see the two-legged thermoelectric generator which consists of a MoS_2 and ZnO leg at 310K.

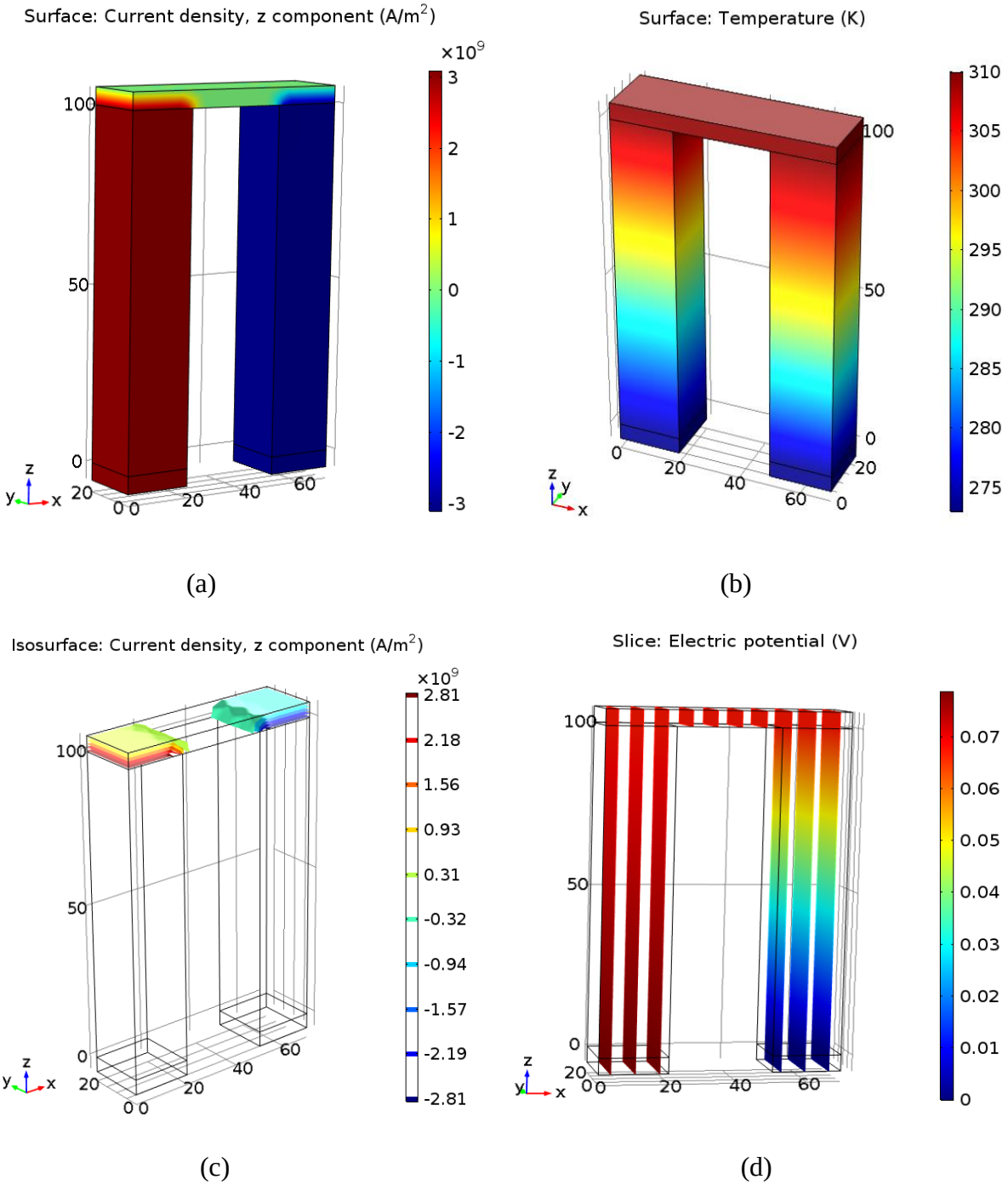

Figure19. (a) Current Density of MoS_2 and ZnO using surface area. (b) Temperature of MoS_2 and ZnO. (c) Current Density of MoS_2 and ZnO using Isosurface (d) Electric potential using Slice at 310K.

The contact on the TEG was made of Copper. The main objective of this study is to measure the potential across the two legs of the generator and also the surface current that it can produce. We will also look at the direction of current flow. From the figure (19), we can see that the highest electric potential is $78.91 \times 10^{-3}V$. From the figure (19), we can also see that the current density is at $2.78 \times 10^{9}Am^{-2}$.

.

7.0 Conclusion:

The above design and analysis shows that there is a linearly decreasing order or electrical conductivity due to increase of temperature. And since the figure of merit is (1) depends on Seebeck, Electrical conductivity and Thermal conductivity. Therefore, if the Seebeck and electrical conductivity values are increased and thermal conductivity values are decreased then the figure of merit will increase. Therefore, we can say that the relation between figure of merit (ZT) is inversely proportional to the thermal conductivity. All the materials that we have analyzed in the above section give the highest ZT value in their respective room temperatures.

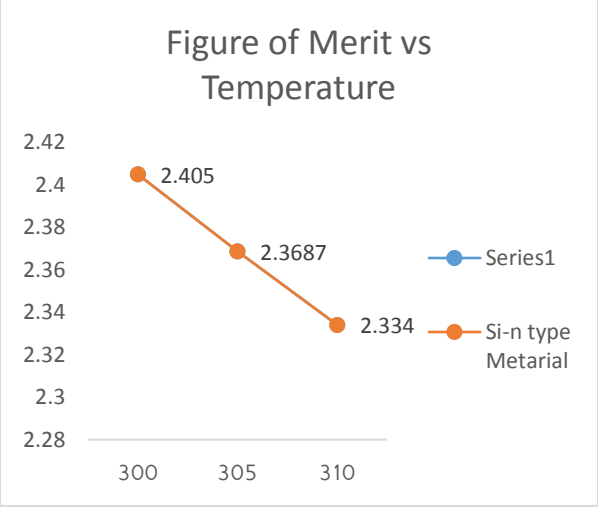

(a)

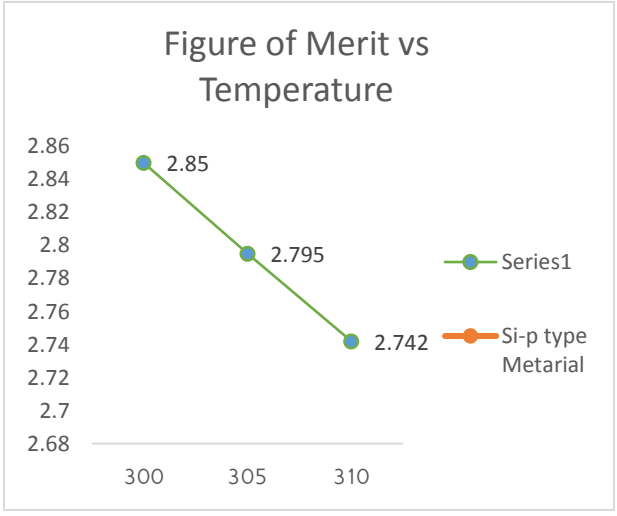

(b)

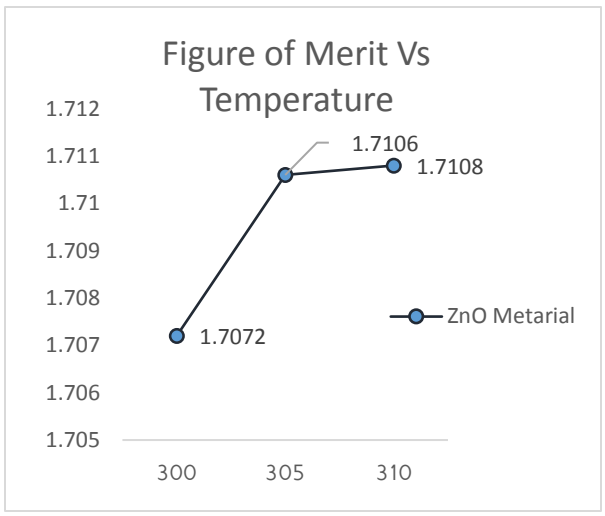

(c)

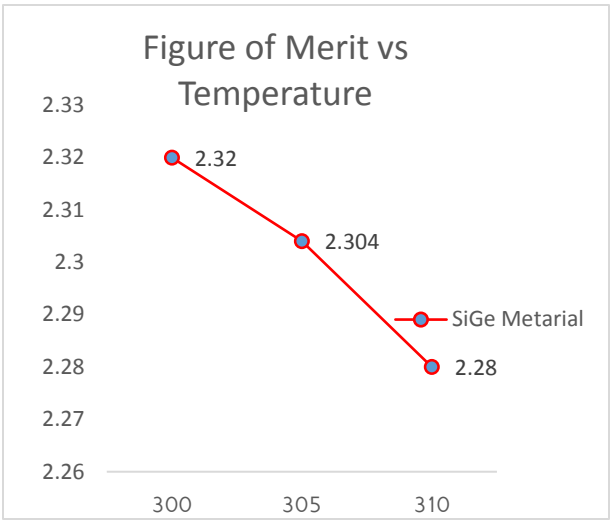

(d)

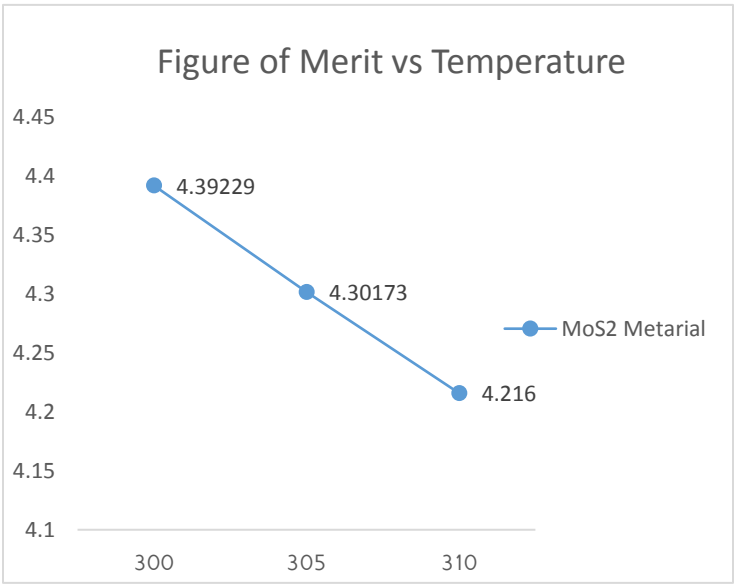

(e)

Figure 20. Figure of Merit Vs Temperature –

(a) Si-n Type (b) Si-p Type (c) ZnO (d) SiGe (e) MoS_2

The figure (20) shows that Si-n type gets highest ZT value of 2.405 at 300K, Si-p type gets highest ZT value of 2.85 at 300K, ZnO gets highest ZT of 1.7108 at 310K, SiGe gets highest ZT value of 2.32 at 300K and MoS_2 gets highest ZT value of 4.3929 at 300K. So, we can see that the MoS_2 gives the highest value of ZT at conventional room temperature(300K). We get the electric potential value $78.9 \times 10^{-3} V$ in MoS_2 -ZnO based TEG. Furthermore, Si-n type based one legged TEG produced the highest current density value of $1.632 \times 10^{11} Am^{-2}$. From all these analyses we have come to the decision that the Seebeck effect that is responsible for the thermoelectricity is inversely proportional to the thermal conductivity. This infact exhibits the property of the materials such that we can say, the current density throught a thermoelectric material is best when the Seebeck co-efficient is high, the electrical conductivity is high while the thermal conductivity is low. Therefore, to refine the results for enhanced performance and resolve the issue at hand, reduction of thermal conductivity will be very important.

References

[1] J. Zheng, "Recent advances on thermoelectric materials," Frontiers of Physics in China, vol. 3, no. 3, pp. 269–279, Jul. 2008.

[2] "Basic research needs for solar energy utilization", Report of the basic energy sciences workshop on solar energy utilization, April 18-21, 2005. DOE, USA.

[3] H. J. Goldsmid, (1986) Electronic Refrigeration (Pion, London), p.10.

[4] G. D. Mahan, and J. O. Sofo, Proc. Natl. Acad. Sci. USA, 1996, 93: 7436

[5] Z.-G. Chen, G. Han, L. Yang, L. Cheng, and J. Zou, "Nanostructured thermoelectric materials: Current research and future challenge," Progress in Natural Science: Materials International, vol. 22, no. 6, pp. 535–549, Dec. 2012.

[6] J.R. Sootsman, D.Y. Chung, M.G. Kanatzidis, New and old concepts in thermoelectric materials, Angewandte Chemie, International Edition 48 (2009) 8616–8639.

[7] C.J. Vineis, A. Shakouri, A. Majumdar, M.G. Kanatzidis, Nanostructured thermoelectrics: big efficiency gains from small features, Advanced Materials 22 (2010) 3970–3980.

[8] P. Vaqueiro, A.V. Powell, Recent developments in nanostructured materials for high-performance thermoelectrics, Journal of Materials Chemistry 20 (2010) 9577–9584.

[9] S.K. Bux, J.P. Fleurial, R.B. Kaner, Nanostructured materials for thermoelectric applications, Chemical Communications 46 (2010) 8311–8324.

[10] G.J. Snyder, E.S. Toberer, Complex thermoelectric materials, Nature Materials 7 (2008) 105–114.

[11] A.J. Minnich, M.S. Dresselhaus, Z.F. Ren, G. Chen, Bulk nanostructured thermoelectric materials: current research and future prospects, Energy & Environmental Science 2 (2009) 466–479.

[12] M.G. Kanatzidis, Nanostructured thermoelectrics: the new paradigm?, Chemistry of Materials 22 (2009) 648–659.

[13] D.L. Medlin, G.J. Snyder, Interfaces in bulk thermoelectric materials: a review for current opinion in colloid and interface science, Current Opinion in Colloid & Interface Science 14(2009) 226–235.

[14] P. Pichanusakorn, P. Bandaru, Nanostructured thermoelectrics, Materials Science and Engineering: R: Reports 67 (2010) 19–63.

[15] M. Zebarjadi, K. Esfarjani, M.S. Dresselhaus, Z.F. Ren, G. Chen, Perspectives on thermoelectrics: from fundamentals to device applications, Energy & Environmental Science 5 (2012) 5147–5162.

[16] C. Wood, Rep. Prog. Phys., 1988, 51: 459

[17] F. R. Stabler, Mater. Res. Soc. Symp. Proc. Vol. 886, 2006 # 0886-F01-04.1

[18] M.S. Dresselhaus, G. Chen, M.Y. Tang, R.G. Yang, H. Lee, D.Z. Wang, et al., New directions for low-dimensional thermoelectric materials, Advanced Materials 19 (2007) 1043–1053.

[19] G.A. Slack, in: M. Rowe (Ed.), CRC Handbook of Thermoelectrics, CRC Press, Boca Raton, FL, 1995.

[20] J.R. Szczech, J.M. Higgins, S. Jin, Enhancement of the thermoelectric properties in nanoscale and nanostructured materials, Journal of Materials Chemistry 21 (2011) 4037–4055.

[21] G. D. Mahan, and J. O. Sofo, Proc. Natl. Acad. Sci. USA, 1996, 93: 7436

[22] Z. Tian, S. Lee, and G. Chen, "COMPREHENSIVE REVIEW OF HEAT TRANSFER IN THERMOELECTRIC MATERIALS AND DEVICES," Annual Review of Heat Transfer, vol. 17, no. N/A, pp. 425–483, 2014.

[23] S. L. Dudarev, G. A. Botton, S. Y. Savrasov, C. J. Humphreys, and A. P. Sutton, Phys. Rev. B, 57, 1505,1998.

[24] M. Cococcioni, and S. de Gironcoli, Phys. Rev. B, 71, 35105, 2005

[25] "ATK version 2015.1", QuantumWise A/S (www.quantumwise.com).

[26] B.C. Sales, D. Mandrus, B.C. Chakoumakos, V. Keppens, J.R. Thompson, Filled skutterudite antimonides: Electron crystals and phonon glasses, Physical Review B 56 (1997) 15081.

[27] B.C. Sales, D. Mandrus, R.K. Williams, Filled skutterudite antimonides: a new class of thermoelectric materials, Science

(New York, NY) 272 (1996) 1325–1328.

[28] G.S. Nolas, M. Kaeser, R.T. Littleton, T.M. Tritt, High figure of merit in partially filled ytterbium skutterudite materials, Applied Physics Letters 77 (2000) 1855–1857.

[29] T. He, J. Chen, H.D. Rosenfeld, M.A. Subramanian, Thermo- electric properties of indium-filled skutterudites, Chemistry of Materials 18 (2006) 759–762.

[30] W.S. Liu, B.P. Zhang, L.D. Zhao, J.F. Li, Improvement of thermoelectric performance of CoSb (3?x) Te (x) skutterudite compounds by additional substitution of IVB-group elements for Sb, Chemistry of Materials 20 (2008) 7526–7531.

[31] X. Shi, J. Yang, S. Bai, J. Yang, H. Wang, M. Chi, et al., On the design of high-efficiency thermoelectric clathrates through a systematic cross-substitution of framework elements, Advanced Functional Materials 20 (2010) 755–763.

[32] Y. Liu, L.M. Wu, L.H. Li, S.W. Du, J.D. Corbett, L. Chen, The antimony-based type I clathrate compounds Cs (8) Cd (18) Sb (28) and Cs (8) Zn (18) Sb (28) , Angewandte Chemie, International Edition 48 (2009) 5305–5308.

[33] C.L. Condron, S.M. Kauzlarich, F. Gascoin, G.J. Snyder, Thermoelectric properties and microstructure of Ba 8 Al 14 Si 31 and EuBa 7 Al 13 Si 33, Chemistry of Materials 18 (2006) 4939–4945.

[34] H. Kleinke, New bulk materials for thermoelectric power generation: clathrates and complex antimonides, Chemistry of Materials 22 (2010) 604–611.

[35] J. Androulakis, C.H. Lin, H.J. Kong, C. Uher, C.I. Wu, T. Hogan, et al., Spinodal decomposition and nucleation and growth as a means to bulk nanostructured thermoelectrics: enhanced performance in Pb_{1-x} Sn_x-TePbS, Journal of the American Chemical Society 129 (2007) 9780–9788.

[36] G.J. Snyder, E.S. Toberer, Complex thermoelectric materials, Nature Materials 7 (2008) 105–114.

[37] B.B. Iversen, Fulfilling thermoelectric promises: beta-Zn 4 Sb 3 from materials research to power generation, Journal of Materials Chemistry 20 (2010) 10778–10787.

[38] W. Zhao, P. Wei, Q. Zhang, C. Dong, L. Liu, X. Tang, Enhanced thermoelectric performance in barium and indium double-filled skutterudite bulk materials via orbital hybridization induced by indium filler, Journal of the American Chemical Society 131 (2009) 3713–3720.

[39] H. Li, X.F. Tang, X.L. Su, Q.J. Zhang, Preparation and thermoelectric properties of high-performance Sb additional Yb (0.2) Co (4) Sb (12þy) bulk materials with nanostructure, Applied Physics Letters 92 (2008) 202114.

[40] H. Li, X.F. Tang, Q.J. Zhang, C. Uher, Rapid preparation method of bulk nanostructured Yb (0.3) Co (4) Sb (12þy) compounds and their improved thermoelectric performance, Applied Physics Letters 93 (2008) 202114.

[41] Y.Z. Pei, J. Yang, L.D. Chen, W. Zhang, J.R. Salvador, J.H. Yang, Improving thermoelectric performance of caged compounds through light-element filling, Applied Physics Letters 95 (2009) 042101.

[42] J.L. Mi, T.J. Zhu, X.B. Zhao, J. Ma, Nanostructuring and thermoelectric properties of bulk skutterudite compound CoSb 3, Journal of Applied Physics 101 (2007) 054314.

[43] X. Shi, J. Yang, J.R. Salvador, M. Chi, J.Y. Cho, H. Wang, et al., Multiple-filled skutterudites: High thermoelectric figure of merit through separately optimizing electrical and thermal transports, Journal of the American Chemical Society 133 (2011) 7837–7846.

[44] A. Saramat, G. Svensson, A.E.C. Palmqvist, C. Stiewe, E. Mueller, D. Platzek, et al., Large thermoelectric figure of merit at high temperature in Czochralski-grown clathrate Ba8Ga16Ge30, Journal of Applied Physics 99 (2006) 023708.

[45] L.D. Hicks, M.S. Dresselhaus, Thermoelectric figure of merit of a one-dimensional conductor, Physical Review B 47 (1993) 16631–16634.

[46] X.B. Zhao, X.H. Ji, Y.H. Zhang, T.J. Zhu, J.P. Tu, X.B. Zhang, Bismuth telluride nanotubes and the effects on the thermoselectric properties of nanotube-containing nanocomposites, Applied Physics Letters 86 (2005) 062111.

[47] G. Zhang, Q. Yu, W. Wang, X. Li, Nanostructures for thermo-electric applications: synthesis, growth mechanism, and property studies, Advanced Materials 22 (2010) 1959–1962.

[48] A.I. Hochbaum, R. Chen, R.D. Delgado, W. Liang, E.C. Garnett, M. Najarian, et al., Enhanced thermoelectric performance of rough silicon nanowires, Nature 451 (2008) 163–U165.

[49] A.I. Boukai, Y. Bunimovich, J. Tahir-Kheli, J.-K. Yu, W.A. Goddard III, J.R. Heath, Silicon nanowires as efficient thermoelectric materials, Nature 451 (2008) 168–171.

[50] A.I. Persson, Y.K. Koh, D.G. Cahill, L. Samuelson, H. Linke, Thermal conductance of InAs nanowire composites, Nano Letters 9 (2009) 4484–4488.

[51] A. Mavrokefalos, A.L. Moore, M.T. Pettes, L. Shi, W. Wang, X. Li, Thermoelectric and structural characterizations of individual electrodeposited bismuth telluride nanowires, Journal of Applied Physics 105 (2009) 104318.

[52] F. Zhou, J.H. Seol, A.L. Moore, L. Shi, Q.L. Ye, R. Scheffler, One-dimensional electron transport and thermopower in an individual InSb nanowire, Journal of Physics: Condensed Matter 18 (2006) 9651–9657.

[53] F. Zhou, A.L. Moore, M.T. Pettes, Y. Lee, J.H. Seol, Q.L. Ye, et al., Effect of growth base pressure on the thermoelectric properties Nanostructured thermoelectric materials: Current

research and future challenge 547 of indium antimonide nanowires, Journal of Physics D: Applied Physics 43 (2010) 025406.

[54] C.J. Vineis, A. Shakouri, A. Majumdar, M.G. Kanatzidis, Nanostructured thermoelectrics: big efficiency gains from small features, Advanced Materials 22 (2010) 3970–3980.

[55] L.D. Hicks, M.S. Dresselhaus, Effect of quantum-well structures on the thermoelectric figure of merit, Physical Review B 47 (1993) 12727.

[56] R. Venkatasubramanian, E. Siivola, T. Colpitts, B. O'Quinn, Thin-film thermoelectric devices with high room-temperature figures of merit, Nature 413 (2001) 597–602.

[57] T.C. Harman, P.J. Taylor, M.P. Walsh, B.E. LaForge, Quantum dot super lattice thermoelectric materials and devices, Science (New York, NY) 297 (2002) 2229–2232.

[58] I. Chowdhury, R. Prasher, K. Lofgreen, G. Chrysler, S. Narasimhan, R. Mahajan, et al., On-chip cooling by superlattice-based thin-film thermoelectrics, Nature Nanotechnology 4 (2009) 235–238.

[59] J.J. Urban, D.V. Talapin, E.V. Shevchenko, C.R. Kagan, C.B. Murray, Synergism in binary nanocrystal super lattices leads to enhanced p-type conductivity in self-assembled PbTe/ Ag-2 Te thin films, Nature Materials 6 (2007) 115–121.

[60] L.D. Hicks, T.C. Harman, X. Sun, M.S. Dresselhaus, Experimental study of the effect of quantum-well structures on the thermoelectric figure of merit, Physical Review B 53 (1996) R10493.

[61] E.I. Rogacheva, O.N. Nashchekina, A.V. Meriuts, S.G. Lyubchenko, M.S. Dresselhaus, G. Dresselhaus, Quantum size effects in n-PbTe/p-SnTe/n-PbTe heterostructures, Applied Physics Letters 86 (2005) 063103.

[62] A. Shakouri, Thermoelectric, thermionic and thermos photovoltaic energy conversion, Proceedings of the International Conference on Thermoelectrics (2005) 492–497.

[63] C.J. Vineis, A. Shakouri, A. Majumdar, M.G. Kanatzidis, Nanostructured thermoelectrics: big efficiency gains from small features, Advanced Materials 22 (2010) 3970–3980.

[64] J.R. Szczech, J.M. Higgins, S. Jin, Enhancement of the thermoelectric properties in nanoscale and nanostructured materials, Journal of Materials Chemistry 21 (2011) 4037–4055.

[65] S. Datta, *Lessons from Nanoelectronics: A new perspective on transport*, Second Edition ed. Singapore, Singapore: World Scientific Publishing Co Pte, 2012.

[66] M. Lundstrom and C. Jeong, *Near-equilibrium transport: Fundamentals and applications*, Second ed. Singapore, Singapore: World Scientific Publishing Co Pte, 2013.